AEROELASTIC ANALYSIS OF SMALL-SCALE AIRCRAFT

A Thesis

presented to

the Faculty of California Polytechnic State University,

San Luis Obispo

In Partial Fulfillment

of the Requirements for the Degree

Master of Science in Aerospace Engineering

by

Kent Roberts

January 2022

COMMITTEE MEMBERSHIP

TITLE:	Aeroelastic Analysis of Small-Scale Aircraft
AUTHOR:	Kent Roberts
DATE SUBMITTED:	January 2022
COMMITTEE CHAIR:	Arnold Deffo, Ph.D. Assistant Professor of Aerospace Engineering
COMMITTEE MEMBER:	Aaron Drake, Ph.D. Professor of Aerospace Engineering
COMMITTEE MEMBER:	Paulo Iscold, Ph.D. Associate Professor of Aerospace Engineering
COMMITTEE MEMBER:	Walter Silva, Ph.D. Senior Research Scientist - NASA Langley

ABSTRACT

Aeroelastic Analysis of Small-Scale Aircraft

Kent Roberts

The structural design of flight vehicles is a balancing act between maximizing loading capability while minimizing weight. An engineer must consider not only the classical static structural yielding failure of a vehicle, but a variety of ways in which structural deformations can in turn, affect the loading conditions driving those deformations. Lift redistribution, divergence, and flutter are exactly such dynamic aeroelastic phenomena that must be properly characterized during the design of a vehicle; to do otherwise is to risk catastrophe. Relevant within the university context is the design of small-scale aircraft for student projects and of particular consideration, the DBF competition hosted by AIAA. This work implements a variety of aeroelastic analysis methods: K and PK with Theodorsen aerodynamics via Matlab, NASA EZASE, and the FEMAP NX NASTRAN Aeroelasticity Package. These techniques are applied to a number of baseline test cases in addition to two representative DBF wings. Both wings considered ultimately indicated stability within reasonable flight conditions, although each for a different reason. Analysis results for the Cal Poly 2020 wing, a spar-rib construction emblematic of the collocation design approach, showed that the wing was stable within expected flight regions. The USC 2020 wing model, a composite top spar construction, exhibited unstable behavior, however this was well outside the scope of expected flight conditions. The codebase developed as a part of this work will serve as a foundation for future student teams to perform aeroelastic analyses of their own and support continued aeroelastic research at Cal Poly - SLO.

TABLE OF CONTENTS

LIST OF TABLES

LIST OF FIGURES

Nomenclature

μ	mass ratio
ω	circular frequency
ρ	density
σ	ratio of uncoupled frequencies for bending and torsion
AR	aspect ratio
b	semi-chord of wing strip
CG	Center of gravity / center of mass location
CP	Center of pressure / aerodynamic center location
EA	Elastic axis location
EI	bending rigidity
GJ	torsional rigidity
I_p	second polar area moment of inertia
L	lift
$l_w, l_\theta, m_w, m_\theta$	aerodynamic coefficients
M	mach number
q	dynamic pressure
r	dimensionless radius of gyration

U velocity

V reduced velocity

V_{ne} Velocity - Never Exceed

x_θ static-unbalance

Chapter 1

INTRODUCTION

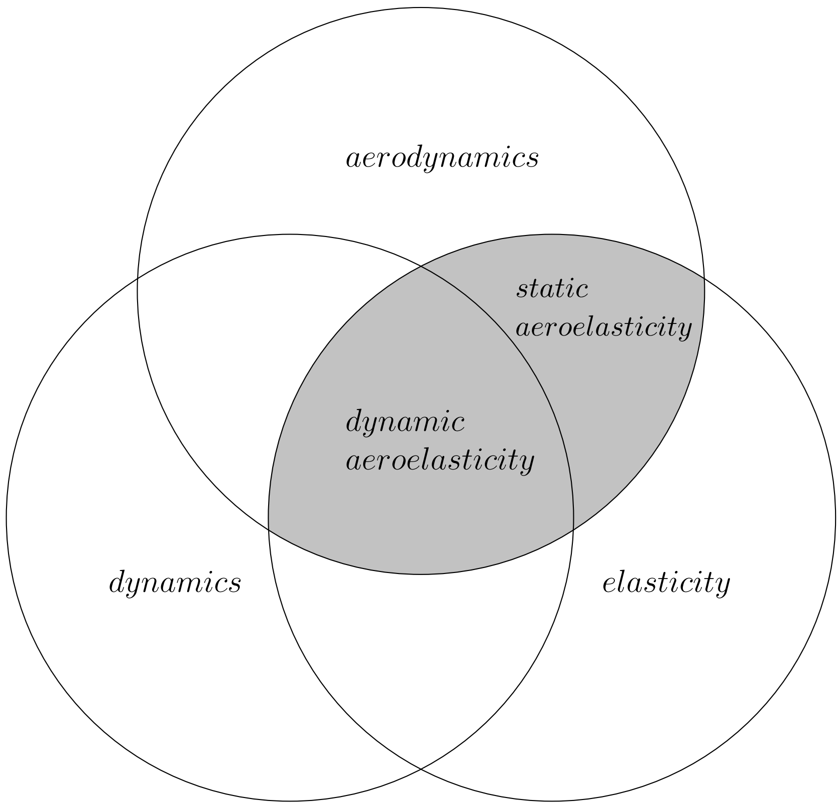

Figure 1.1: Aeroelasticity and related fields [1]

Flight vehicles fundamentally pose a design challenge of optimizing structures to endure flight loads while minimizing weight. Aeroelasticity is the study of how structures deform within a flow medium, encompassing the fields of both structural dynamics and aerodynamics. Figure 1.1, attributed to Professor A. R. Collar in the 1940s is commonly used as an introduction to this branch of study [1]. Fundamentally, aeroelastic phenomena such as lift-redistribution, torsional divergence, and flutter are characterized by the coupling of aerodynamic forces and the deformations driven by those forces. For example, one could imagine a local twist in an airofoil's angle of attack which could in turn increase that driving moment until an equilibrium is reached; in fact, this is an aspect of lift-redistribution.

Aeroelastic phenomena are generally divided into two categories; static and dynamic. As implied, static phenomena are considered independent of time, while dynamic phenomena evolve with time. Perhaps the most fundamental behavior to consider is the redistribution of lift based on structural deformations of a wing. As a wing twists and bends, the effective angle of attack will vary as a function of span-wise location, and thus in-turn changing the aerodynamic behavior of the wing. When the aerodynamic forces and their structural reactions balance, a wing can be considered stable.

Divergence is a static aeroelastic phenomena that naturally follows from lift redistribution. When aerodynamic load builds up in such magnitude to overcome the structural rigidity of a wing, it will fail. Within the analytical theory this commonly manifests as an infinite displacement condition [1]. Torsional divergence (widely considered more common than bending divergence) occurs when the angle of twist at a wing tip tends towards infinity. Note that this failure is distinct from strictly static structural failure which is manifested by the yielding of material (most commonly at the root of a wing where the bending moment is typically at a maximum). Even if divergence is not expected within flight conditions, there are still several ways in which such a structure could experience catastrophic structural failure due to dynamic instability.

The current work will primarily focus on the flutter phenomenon. Flutter is a dynamic aeroelastic condition that arises when a structure extracts energy from the surrounding flow. For flutter to arise, a system usually, although not strictly required, must have more than one degree of freedom and be considered a conservative system within the surrounding flow field [3]. When the phase relationship between the

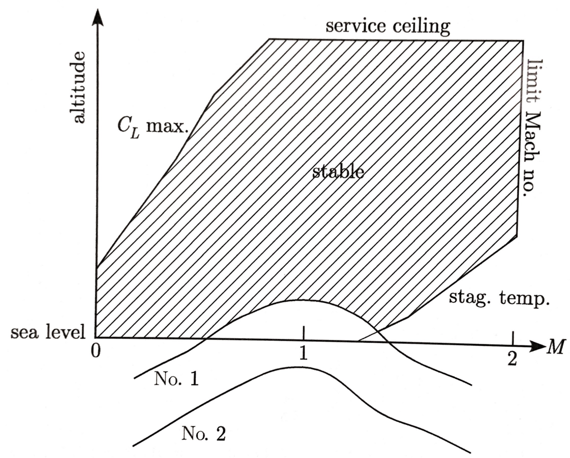

Figure 1.2: Generic flight envelope of a Mach 2 aircraft (Hodges Fig 5.17) [1]

degrees of freedom reaches a sufficient coupling condition, energy absorbed from the flow leads to oscillations. These oscillations become unstable, growing in amplitude until the structural rigidity of the wing is overcome [4]. The speed at which these oscillations change from damped to purely harmonic motion is defined as the flutter speed, beyond which lies conditions of instability and catastrophic failure [1].

The determination of the flutter boundary is a crucial part of defining an aircraft's flight envelope (the region of performance within which an aircraft is safe to operate). A typical flight envelope for a Mach 2 aircraft is included in figure (1.2) [1]. Note the limiting curves, No. 1 (a vehicle susceptible to flutter) and No. 2 (a "flutter-safe" vehicle) represent flutter boundaries, beyond which the vehicle violates the 'flutter safety margin', commonly defined as 15% for US military aircraft and 20% for commercial transport aircraft over the flutter speed [1].

Among the tasks of practicing aeroelasticians is to seek the flutter speed that marks the onset of critical instability for a wide range of flight conditions. Further analysis of sub-critical frequency and damping characteristics can inform modifications, increasing the reliability of the aircraft. A vast collection of both numerical and analytical approaches has been studied as means to determine the flutter boundary, but perhaps the most physical insight is offered via analytical approaches [5].

Historically, flutter was first studied empirically. One of the earliest formulations is attributed to Küssner who observed wing-aileron flutter in 1929 and published a general formula relating critical speed and reduced frequency of a wing [6]. Another major seminal work by Theodorsen (1934) derived an analytical aerodynamic model for thin airfoils oscillating with small amplitudes in incompressible flow [7]. The prevalence of Theodorsen's work in modern literature speaks to its importance as a foundation of the aeroelastic field. Within the near century that has passed since this early work, a vast amount of literature has extended the field. Notably the following texts are keystones of aeroelasticity, levied throughout this project: Bisplinhoff (1962) *Aeroelasticity* [3], Fung (1955) *An Introduction to the Theory of Aeroelasticity* [6], and Hodges (2002) *Introduction to Structural Dynamics and Aeroelasticity* [1].

The primary use of the present work is the completion of aeroelastic studies by university teams within the preliminary and final design phases (such as a part of AIAA's DBF competition). In such a case, many university teams tend to prove out aeroelastic stability via rules of thumb or flight testing, which could pose risk to the project.

Many student designs seek to locate wing elastic axis and center of gravity concentric with the aerodynamic center at the quarter chord location. This is sound in theory as the "less[er] separation between aerodynamic center and structural axis (elastic axis), the lesser the static aeroelastic twist, and higher flutter and divergence air speeds" [8]. However, the effects of aeroelastic phenomena are dictated by more than purely the locations of the elastic, aerodynamic, and mass centers. Great care must always be taken to ensure the structural integrity of aircraft designs.

This work seeks to develop and apply analysis methods to determine the aeroelastic characteristics (flutter speed, divergence dynamic pressure, lift-redistribution) of small (DBF)-scale model aircraft and build a foundation code base for further aeroelastic research at Cal Poly - SLO.

The K and PK methods are implemented within a MatLab environment and compared against NASTRAN NX NASTRAN Aeroelasticy Package finite element method [FEM] commonly used in industry, in addition to the ESAZE code developed for the X-56A [9]. These methods are first compared and validated against Hodges and the EZASE Aluminum beam test case, both fictitious baselines before select combinations of these methods are applied to a sampling of past student DBF wings representing a variety of structural designs.

Chapter 2

METHODOLOGY

2.1 Assumptions

A number of key assumptions can significantly reduce the complexity of the aeroelastic analysis, given the flight conditions of this project's target application.

Compiled in the *AGARD Manual on Aeroelasticity* [4], a collection of parametric studies exist that has established when the following theories apply based on work by Lin, Reissner and Tsien [10], Miles [11], and Landahl, Mollo Christensen and Ashley [12].

2.1.1 Aerodynamic Assumptions

1. **Small disturbances** can be assumed, considering that at the critical condition, the amplitude of the oscillations are small. This is a critical assumption supporting the adoption of linearized aerodynamic theory and linearized elasticity in most cases [6]. Small disturbance theory can be assumed if

$$\delta << 1, \qquad \omega\delta << 1, \qquad M\delta << 1, \qquad M\omega\delta << 1, \tag{2.1}$$

where δl denotes the amplitude of oscillation or thickness of the wing (whichever is larger), and ω the reduced frequency.

2. **Linearization** of the problem is acceptable if any one of the three conditions hold:

$$|M - 1| >> \delta^{2/3}, \qquad \omega >> \delta^{2/3}, \qquad AR << \delta^{-1/3}. \tag{2.2}$$

   A linearized formulation of the problem is critical to apply analytical solution methods.

3. **Incompressible flow** typically can be assumed if [13]:

$$M << 0.3 = 102\, m/s\ (standard\ air). \tag{2.3}$$

   Incompressibility offers significant simplification and holds given the flight regime of student projects.

4. **Thin Airfoil Theory** allows the adoption of lift-curve slope $C_{L_\alpha} = 2\pi[rad^{-1}]$ as opposed to other values (derived from CFD for example) and applies when there exists a small thickness to chord ratio.

2.1.2 Modeling Assumptions

1. **Mode shape truncation** is an important factor when adopting generalized coordinates to describe the total displacement of a structure. Included mode shapes must represent sufficient degrees of freedom to describe relevant total displacements. This is analogous to including sufficient terms in a Fourier series expansion to accurately model a function. The effect of including higher modes can be concluded from the values of the coupling matrix $[A]$. For a homogeneous cantilever wing, Hodges makes the point that including modes beyond the simplest single bending and torsional mode cases only adjust the coupling terms by a factor less than 5% [1].

2. **NASTRAN mesh fidelity** is critically important when constructing finite element models. Setting a good minimum length and considering measures of quality such as the minimum angle, aspect ratio, and Jacobian of elements is typical practice when evaluating the quality of a mesh. For example, the majority of elements which makeup the USC 2020 FEM later considered in the study have a minimum angle in the range $60^\circ - 40^\circ$, and aspect ratio < 3 and a Jacobian > 0.15. Only a high-quality finite element model can be expected to yield accurate models.

2.2 Structure

2.2.1 Boundary Conditions

The wings considered are modeled with fixed-free boundary conditions, typical of a cantilever beam. While body freedom flutter modes are a subject of interest, this study shall not explore such effects, taking the wing-fuselage root attachment to be a rigid boundary condition.

2.2.2 Euler Beam Theory

Structural beam analysis is a well-studied field, with several structural theories relevant to the following regimes. If the ratio of the length to height of a beam, $l/h > 20$ then the beam obeys the simplified kinematic assumptions and it is called an "Euler beam"[14]. Much shorter beams with $l/h < 10$ develop considerable shear stresses in addition to bending stresses and must be treated by a different set of assumptions. Such beams are referred to as Timoshenko beams[14]. The intermediate range

$10 < l/h < 20$ is a grey area where the simplifying assumptions of the elementary beam theory gradually lose validity [14].

Within the relevant context of a wing's aspect ratio and airfoil thickness, Euler beam theory is a sufficient first order approximation and will be adopted in the proceeding analytical studies. However, it is recognized that the finite element method considered via NASTRAN is anticipated to yield more accurate results, hence all relative error will be compared against the finite element results.

2.2.3 Assumed Modes

The assumed modes method is a common foundation of 3D structural dynamics. In the relevant case of a beam in bending and torsion, displacements can generally be represented as separable linear combinations of basis functions:

$$w(y,t) = \sum_{i=1}^{N_w} \eta_i(t)\Psi_i(y), \tag{2.4}$$

$$\theta(y,t) = \sum_{i=1}^{N_\theta} \phi_i(t)\Theta_i(y). \tag{2.5}$$

The mode shapes, Ψ_i and Θ_i are determined by finding the free vibration mode shapes of the structure (in this case a wing) via simulation. For the case of a clamped-free beam, these mode shapes can be represented by [1]:

$$\Theta_i = \sqrt{2}sin\left[\frac{\pi(i-\frac{1}{2})}{l}y\right] \qquad , \qquad i = 1,2,3... \tag{2.6}$$

$$\Psi_i = cosh(\alpha_i y) - cos(\alpha_i y) - \beta_i[sinh(\alpha_i y) - sin(\alpha_i y)] \qquad , \qquad i = 1, 2, 3... \quad (2.7)$$

Values of α_i and β_i are commonly found in reference tables, such as Table 3.1 in Hodges [1].

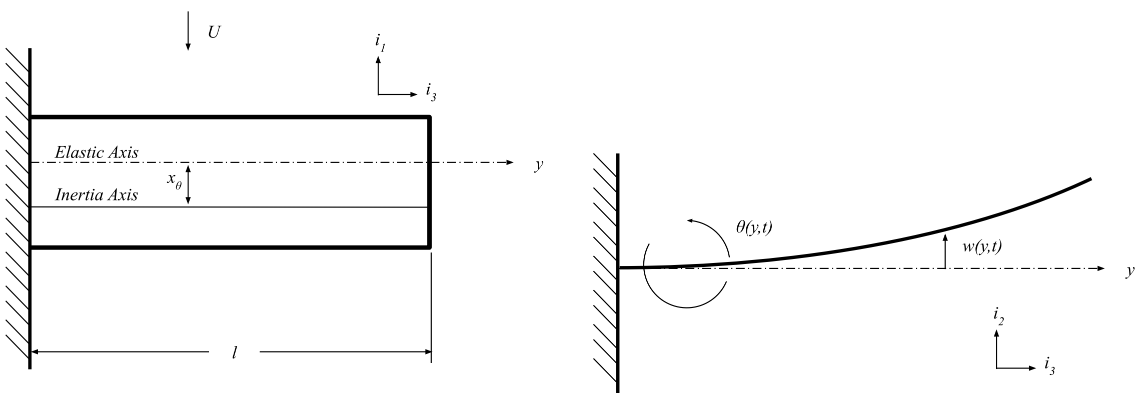

Figure 2.1: Notations for cantilever wing

Additionally, the fundamental bending and torsional frequencies are respectively [1]:

$$\omega_{wi} = (\alpha_i l)^2 \sqrt{\frac{\overline{EI}}{ml^4}} \qquad , \qquad i = 1, 2, 3... \quad (2.8)$$

$$\omega_{\theta i} = \frac{\pi \left(i - \frac{1}{2}\right)}{l} \sqrt{\frac{\overline{GJ}}{Ip}} \qquad , \qquad i = 1, 2, 3... \quad (2.9)$$

Bending and torsional rigidity properties $\overline{EI}$ and $\overline{GJ}$ are to be defined prior to aeroelastic analysis. In addition to the determination of the elastic center, and 2^{nd} polar area moment of area moment of inertia (I_p) which can be non-trivial to determine, especially for non-uniform composite beams considered later.

2.3 Aerodynamics

Aerodynamic theory is a crucial part of aeroelastic analysis. Flutter is inherently a time dependent study, and thus steady aerodynamic theories, while plausible to include in first order approximations, do not completely capture the behavior of the system [1]. Hence, unsteady aerodynamic models must be considered.

Some relevant aerodynamic theories are:

- Prandtl Lifting Line Theory: steady finite span wing - practical for static aeroelastic analysis
- Theodorsen Aerodynamics: harmonically oscillating finite wing - preferred in analytical dynamic aeroelastic analysis
- Doublet Lattice Method (DLM): unsteady 3D panel method - well suited for finite element methods

2.3.1 Prandtl Lifting Line Theory

Within Prandtl lifting line theory, a wing is modeled as a bound vortex located at the quarter chord with an associated shed vortex sheet[15]. The circulation strength of this vortex is taken to be a function of span, thus accounting for the finite ends of the wing [15].

2.3.2 Theodorsen Aerodynamics

In 1936, Theodorsen derived a formulation of the flutter problem assuming a wing of infinite span, small oscillations, within an incompressible and inviscid flow [7]. Given these assumptions, Theodorsen determined the forces and moments on the airfoil via 2D potential flow theory.

Generally, the lift per unit span can be expressed as:

$$L' = -\pi\rho_\infty b^3\omega^2 \left[-l_h(k, M_\infty)\frac{\bar{w}}{b} + l_\theta(k, M_\infty)\bar{\theta} \right], \tag{2.10}$$

and the moment per unit span as:

$$M' = \pi\rho_\infty b^4\omega^2 \left[-m_h(k, M_{\text{inf}})\frac{\bar{w}}{b} + m_\theta(k, M_{\text{inf}})\bar{\theta} \right]. \tag{2.11}$$

Theodorsen limited the above general equations considering only small displacements of a pitching and plunging wings [7]:

$$L'(y,t) = 2\pi\rho_\infty UbC(k) \left[U\theta - \dot{w} + b\left(\frac{1}{2} - a\right)\dot{\theta} \right] + \pi\rho_\infty b^2 \left(U\dot{\theta} - \ddot{w} - ba\ddot{\theta} \right), \tag{2.12}$$

$$M'_{\frac{1}{4}}(y,t) = -\pi\rho_\infty b^3 \left[U\dot{\theta} - \frac{1}{2}\ddot{w} + b\left(\frac{1}{8} - \frac{a}{2}\right)\ddot{\theta} \right]. \tag{2.13}$$

It is convenient to adopt the notation that L_w, L_θ, M_w, M_θ represent the aerodynamic coefficients and are generally dependent on the free stream Mach number M_∞. Considering the incompressibility assumption, these coefficients are only functions of the reduced frequency k.

$$
\begin{aligned}
L_w &= 1 - \frac{2iC(k)}{k} \\
L_\theta &= a + \frac{i}{k}\left[1 + 2\left(\frac{1}{2} - a\right)C(k)\right] + \frac{2C(k)}{k^2} \\
M_w &= \frac{1}{2} \\
M_\theta &= \frac{3}{8} - \frac{i}{k}
\end{aligned}, \tag{2.14}
$$

with $C(k)$ representing the well-known Theodorsen's lift deficiency function[1],

$$
C(k) = \frac{H_1^{(2)}(k)}{H_1^{(2)}(k) + iH_0^{(2)}(k)}, \tag{2.15}
$$

where $H_n^{(2)}(k)$ represents the Hankel function of the second kind of order n.

Note that this theory is complete when implemented within the K-Method which purely considers harmonic motion. Theodorsen aerodynamics is still adopted in the following PK-method presented, representing a hybrid amalgamation of non-harmonic structural motion while still limiting aerodynamic forces to be functions of purely frequency.

2.3.3 Doublet Lattice Method

The doublet lattice method was first introduced by Dr. Edward Albano and Dr. William P. Rodden in 1969 as linearized formulation for oscillating, subsonic lifting surfaces deriving a relationship for the normal velocity at a discrete panel surface to the pressure difference across the surface [16]. In addition to the original work, the 1992 report *A Compilation of the Mathematics Leading to the Doublet Lattice Method* serves as a comprehensive guide to the subject [17]. The following section shall summarize broad strokes of the doublet lattice method, compiled from the two works.

2.3.3.1 Potential Flow

Starting from Euler's five differential equations for inviscid flow equations (one equation of continuity, three equations for momentum, and one state equation), pressure (p) and density (ρ) distributions of the flow domain can be sought as function of velocity potential, ϕ. For the sake of brevity, it serves to adopt an alternative definition of velocity potential[17]:

$$\phi = \Phi - \frac{U^2 t}{2} \tag{2.16}$$

Further, dividing ϕ into two components, a steady state component (bar) and a small disturbance component (tilde) which is time dependent, in addition to a steady state flow field yields the classical linear small disturbance velocity potential partial derivative equation (PDE) [17]:

$$(1 - M^2)\tilde{\phi}_{xx} + \tilde{\phi}_{yy} + \tilde{\phi}_{zz} - \left(\frac{2U}{a_0^2}\right)\tilde{\phi}_{xt} - \left(\frac{1}{a_0^2}\right)\tilde{\phi}_{tt} = 0. \tag{2.17}$$

2.3.3.2 Boundary Conditions

A 3D time variant surface of a wing can be defined as:

$$F_w(x, y, x, t) = z - h_m(x, y, t) \pm h_t(x, y) = 0. \tag{2.18}$$

Where h_t, the thickness of the surface is assumed as a time invariant modification to the mid plane h_m deformations. On the surface boundary the flow is constrained to be purely tangential.

$$\frac{\partial F}{\partial t} + \vec{V} \cdot F = 0. \tag{2.19}$$

2.3.3.3 Acoustic Potential

It can be shown that equation 2.17 takes the form of the classical acoustic equation 2.20 via a coordinate transformation from the (x, y, z) frame to the (x_0, y_0, z_0) frame which moves with the atmosphere at constant velocity $U\hat{i}$ [17].

$$\underline{\phi}_{x_0 x_0} + \underline{\phi}_{y_0 y_0} + \underline{\phi}_{z_0 z_0} - \left[\frac{1}{a^2}\right] \underline{\phi}_{\tau\tau} = 0. \tag{2.20}$$

Thus, it is intuitive to seek elementary solutions to the classical acoustic equation which can be build (incrementally) to represent flows of higher complexity via the principle of super position. Purely modeling a surface as a continuous sheet of source elements is not sufficient to generate a pressure differential across the surface, given the x-y plane symmetry of a source flow. Thus, a new fundamental flow pattern known as the doublet warrants introduction. A doublet is conceptually the limit of two sources of opposite strengths, inversely proportional to the separation between them approach co-location. Such a flow enables discontinuous pressure jumps across a surface and hence, is a favored candidate for elementary functions, combinations of which can be combined to represent lifting surfaces.

It can be shown that the potential function of a doublet ϕ_d [17]

$$\phi_d = \frac{\partial}{\partial z}(\phi_s), \tag{2.21}$$

with ϕ_s represents the potential function of a source element.

For a single oscillating doublet the corresponding potential take the form [17]:

$$\overline{\phi}(x, y, z) = \frac{-1}{U} exp\left[\frac{-i\omega(x-\xi)}{U}\right] \int_{-\infty}^{x-\xi} exp\frac{i\omega\lambda}{U}\overline{\psi}(\lambda, y, z)d\lambda. \tag{2.22}$$

Leveraging this expression, yields an equation for the downwash $\overline{w}$ [17]:

$$\overline{w}(x, y, z) = \left[\frac{-1}{4\pi\rho U}\right] \int\int_S \Delta\overline{p} K((x-\xi), (y-\eta), z) d\xi d\eta. \tag{2.23}$$

where K represents the introduction of the Kernel function [17]:

$$K(x_0, y_0, z_0) = exp\left(\frac{-i\omega x_0}{U}\right) \frac{\partial^2}{\partial z^2}\left[\int_{-\infty}^{x_0} \frac{1}{\overline{R}} exp\left[\frac{i\omega}{U\beta^2}(\lambda - M\overline{R})\right] d\lambda\right], \tag{2.24}$$

with

$$\overline{R} = (\lambda^2 + \beta^2 y_0^2 + \beta^2 z_0^2)^{1/2}. \tag{2.25}$$

Greater simplification is sought for the time begin via the limitation to planar wings, ($z \to 0$) however the partial derivative within the Kernel function must first be evaluated. The Kernel function now ultimately takes the form of [17]:

$$K(x_0, y_0, 0) = \lim_{\epsilon \to 0} \left(\frac{K_1}{y_0^2 + \epsilon^2} \right) exp \left[\frac{-i\omega x_0}{U} \right], \tag{2.26}$$

with

$$K_1 = -I_1 - \left[\frac{M|y_0|}{(x_0^2 + \beta^2 y_0^2)^{1/2}} \right] \left[\frac{exp(-ik_1 u_1)}{(1 + u_1^2)^{1/2}} \right], \tag{2.27}$$

$$I_1 = \int_{u_1}^{\inf} \left[\frac{exp(-ik_1 u)}{(1 + u^2)^{3/2}} \right] du, \tag{2.28}$$

$$k_1 = \frac{\omega |y_0|}{U}, \tag{2.29}$$

$$u_1 = \frac{M(x_0^2 + \beta^2 y_0^2)^{1/2} - x_0}{|y_0| \beta^2}. \tag{2.30}$$

Note a variety of singularities may occur when $y_0 \to 0$, $y = \eta$, $x_0 = y_0$, etc. The doublet lattice approximation (for which this method derives its name) is an empirical approximation to evaluate the integrals of equations 2.27 through 2.30. The continuous doublet sheet (equation 2.23) is replaced by a set of finite length pressure doublet lines located at 1/4 chord of each panel as in figure 2.2.

The quarter chord location is arbitrarily defined but a widely accepted position to locate the doublet lines. Ultimately further reduction yields a relationship between the downwash $\overline{w}$ and the pressure differential Δp of another element. Implementing a summation of the effects across all panels, the downwash at a $(x, y, 0)$ location due to N_x by N_y number of discretized panels

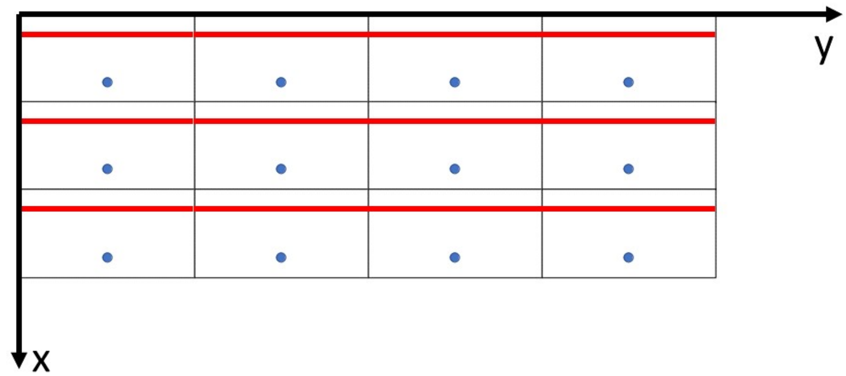

Figure 2.2: A rectangular wing divided into $N_x = 3$ by $N_y = 4$ panels with $1/4$ chord doublet lines marked in red and $3/4$ chord locations in blue

$$\overline{w}(x, y, 0) = \left[\frac{1}{4\pi\rho U}\right] \sum_{i=1}^{N_x} \sum_{j=1}^{N_y} [-\Delta p_{ij} \Delta\eta_{ij}][B_0(x_i, y_j) + B_1(x_i, y_j) + B_2(x_i, y_j)]. \quad (2.31)$$

Evaluating equation 2.31 at 3/4 chord of each for each panel element and noting the surface tangential flow constraint (downwash, $w = 0$ or a non-zero relative motion if the panel is in motion) yields an $N_x + N_y$ set of equations with $N_x + N_y$ unknown pressure differentials across each element.

Relating the pressure differential into terms of generalized forces is carried out via

$$\{F\}_{AIC} = \frac{1}{2}\left(\frac{\rho}{\rho_0}\right)\rho_0 U^2 [B][D]^{-1}[W]\{h\}, \quad (2.32)$$

where $\{h\}$ is the vector of generalized structural coordinates, $[W]$ maps the degrees of freedom of the structural model to the aerodynamic control points of the aerodynamic model (within FEMAP NX NASTRAN this concept is represented by "splines"), $[D]^{-1}$ relates the downwash to the non-dimensional relative pressure across each panel, and $[B]$ that represents the integration of the pressures on each panel into forces and moments on the structural model [18].

The doublet lattice method is impractical to implement by hand and hence better suited for computation codes. The development of such codes represents significant effort within the aerospace industry. Of note is that, although limited **H7WC** was one of the first widely adopted DLM codes created by Douglas, Long Beach, California [19]. The exact code included in the FEMAP NX NASTRAN Aeroelasticity page is proprietary although the user manual does suggest the DLM implementation is based on the **N5KA** code developed by Giesing et al. with at the Air Force Flight Dynamics Laboratory [20].

2.4 Flutter Solution Methods

A number of solution techniques have been developed to address the flutter problem. Initially methods considered purely oscillatory behavior represented by reduced frequency k. Historically, a number of studies considered including a correctional term for structural damping via a term 'g'. Flutter occurs when $g = 0$ or close to the actual structural damping. This gave rise to the ubiquitous $V - g$ plotting technique. In which the damping of various mode shapes are plotted against free stream velocity. Note that both normalized, and non-normalized depictions of this data is common throughout the literature. This work favors presenting the full dimensional values.

The p-method is a relaxation of the k-method, now considering non-harmonic motion. However, modern techniques often favor finite element methods such as included in the FEMAP NX NASTRAN Aeroelasticity package for their robust broad applicability.

Throughout, it is convenient to operate with the following reduced set of variables (matching Hodges):

$$\begin{aligned} r^2 &= \frac{Ip}{mb^2} \quad , \quad \sigma = \frac{\omega_h}{\omega_\theta} \\ \mu &= \frac{m}{\rho_\infty \pi b^2} \quad , \quad V = \frac{U}{b\omega_\theta} \\ x_\theta &= e - a \quad , \quad \nu = \frac{pU}{b}, \end{aligned} \tag{2.33}$$

where:

- r represents the dimensionless radius of gyration of the section
- σ denotes the ratio of uncoupled frequencies for bending and torsion
- μ is the mass ratio; and V represents the reduced velocity
- x_θ is the static-unbalance
- p (the name sake of this method) represents a dimensionless unknown variable defined relative to ν

2.4.1 K-Method

The K-Method operates under the assumption that the wings act in purely oscillatory motion. This is true only for the onset of flutter when the damping term goes to zero.

Starting from Hodges Equations 5.129 for the generalized forces using Theodorsen aerodynamics:

$$
\begin{Bmatrix} \Xi_w \\ \Xi_\theta \end{Bmatrix} = -\pi\rho_\infty b^2 l \begin{bmatrix} [\Delta] & ba[A]^T \\ ba[A] & b^2(a^2+\frac{1}{8})[\Delta] \end{bmatrix} \begin{bmatrix} \ddot{\eta} \\ \ddot{\zeta} \end{bmatrix}
$$

$$
-\pi\rho_\infty bUl \begin{bmatrix} 2C(k)[\delta] & -b[1+2(\frac{1}{2}-a)C(k)][A]^T \\ 2b(\frac{1}{2}+a)C(k)[A] & b^2(\frac{1}{2}-a)[1-2(\frac{1}{2}+a)C(k)][\Delta] \end{bmatrix} \begin{bmatrix} \dot{\eta} \\ \dot{\zeta} \end{bmatrix}. \qquad (2.34)
$$

$$
-\pi\rho_\infty bU^2 l \begin{bmatrix} [0] & -2C(k)[A]^T \\ [0] & -b(1+2a)C(k)[\Delta] \end{bmatrix} \begin{bmatrix} \eta \\ \zeta \end{bmatrix}
$$

To condense notation take:

$$
\begin{Bmatrix} \Xi_w \\ \Xi_\theta \end{Bmatrix} = -\pi\rho_\infty b^2 l \begin{bmatrix} Th_1 \end{bmatrix} \begin{bmatrix} \ddot{\eta} \\ \ddot{\zeta} \end{bmatrix} - \pi\rho_\infty bUl \begin{bmatrix} Th_2 \end{bmatrix} \begin{bmatrix} \dot{\eta} \\ \dot{\zeta} \end{bmatrix} - \pi\rho_\infty bU^2 l \begin{bmatrix} Th_3 \end{bmatrix} \begin{bmatrix} \eta \\ \zeta \end{bmatrix}, \qquad (2.35)
$$

and the corresponding equations of motion from Hodges 5.130

$$
ml \begin{bmatrix} [\Delta] & -bx_\theta[A]^T \\ -bx_\theta[A] & b^2r^2[\Delta] \end{bmatrix} \begin{bmatrix} \ddot{\eta} \\ \ddot{\zeta} \end{bmatrix} + \begin{bmatrix} \frac{EI}{l^3}[B] & [0] \\ [0] & \frac{GJ}{l}[T] \end{bmatrix} \begin{bmatrix} \eta \\ \zeta \end{bmatrix} = \begin{Bmatrix} \Xi_w \\ \Xi_\theta \end{Bmatrix} \qquad (2.36)
$$

$$
ml \begin{bmatrix} M \end{bmatrix} \begin{bmatrix} \ddot{\eta} \\ \ddot{\zeta} \end{bmatrix} + \begin{bmatrix} K \end{bmatrix} \begin{bmatrix} \eta \\ \zeta \end{bmatrix} = \begin{Bmatrix} \Xi_w \\ \Xi_\theta \end{Bmatrix}. \qquad (2.37)
$$

Now, considering the generalized coordinates to be exponential functions representing purely harmonic motion of the form:

$$
\eta_i(t) = \bar{\eta}_i exp(i\omega t) \qquad (2.38)
$$

$$\zeta_i(t) = \bar{\zeta}_i exp(i\omega t), \tag{2.39}$$

the differential terms become:

$$\dot{\eta}_i = i\omega\bar{\eta}_i exp(i\omega t), \qquad \dot{\zeta}_i = i\omega\bar{\zeta}_i exp(i\omega t),$$
$$\ddot{\eta}_i = -\omega^2\bar{\eta}_i exp(i\omega t), \qquad \ddot{\zeta}_i = -\omega^2\bar{\zeta}_i exp(i\omega t).$$

The equations of motion reduce to:

$$\pi\rho_\infty b^2 l \begin{bmatrix} Th_1 \end{bmatrix} \omega^2 - \pi\rho_\infty bUl \begin{bmatrix} Th_2 \end{bmatrix} i\omega - \pi\rho_\infty bU^2 l \begin{bmatrix} Th_3 \end{bmatrix} = ml \begin{bmatrix} M \end{bmatrix} \omega^2 + \begin{bmatrix} K \end{bmatrix}. \tag{2.40}$$

Multiplying all by $\frac{1}{U^2}$ to get

$$\pi\rho_\infty l \begin{bmatrix} Th_1 \end{bmatrix} \frac{b^2\omega^2}{U^2} - \pi\rho_\infty l \begin{bmatrix} Th_2 \end{bmatrix} i\frac{b\omega}{U} - \pi\rho_\infty bl \begin{bmatrix} Th_3 \end{bmatrix} = ml \begin{bmatrix} M \end{bmatrix} \frac{\omega^2}{U^2} + \frac{1}{U^2} \begin{bmatrix} K \end{bmatrix}. \tag{2.41}$$

Using the definition of reduced frequency $k = \frac{b\omega}{U}$ and further reduction yields:

$$\pi\rho_\infty l \begin{bmatrix} Th_1 \end{bmatrix} k^2 - \pi\rho_\infty l \begin{bmatrix} Th_2 \end{bmatrix} ik - \pi\rho_\infty bl \begin{bmatrix} Th_3 \end{bmatrix} = \frac{ml}{b^2} \begin{bmatrix} M \end{bmatrix} k^2 + \frac{1}{U^2} \begin{bmatrix} K \end{bmatrix}. \tag{2.42}$$

Note that for a cantilever beam the stiffness matrix can be reduced in terms of modal frequencies:

$$[K] = ml \begin{bmatrix} [\omega_{w_i}^2] & [0] \\ [0] & b^2 r^2 [\omega_{\theta_i}^2] \end{bmatrix} = ml \begin{bmatrix} \omega \end{bmatrix}. \tag{2.43}$$

Incorporating this and further reduction also using the dimensionless mass ratio μ:

$$\pi\rho_\infty l \begin{bmatrix} Th_1 \end{bmatrix} k^2 - \pi\rho_\infty l \begin{bmatrix} Th_2 \end{bmatrix} ik - \pi\rho_\infty bl \begin{bmatrix} Th_3 \end{bmatrix} = \frac{ml}{b^2} \begin{bmatrix} M \end{bmatrix} k^2 + \frac{ml}{U^2} \begin{bmatrix} \omega \end{bmatrix}. \tag{2.44}$$

Multiplying all by b^2/ml:

$$\frac{b^2\pi\rho_\infty}{m} \begin{bmatrix} Th_1 \end{bmatrix} k^2 - \frac{b^2\pi\rho_\infty}{m} \begin{bmatrix} Th_2 \end{bmatrix} ik - \frac{b^2\pi\rho_\infty}{m} b \begin{bmatrix} Th_3 \end{bmatrix} = \begin{bmatrix} M \end{bmatrix} k^2 + \frac{b^2}{U^2} \begin{bmatrix} \omega \end{bmatrix}. \tag{2.45}$$

Adopting the reduced mass variable $\mu = \frac{m}{\pi\rho_\infty b^2}$:

$$\begin{bmatrix} Th_1 \end{bmatrix} k^2 - \begin{bmatrix} Th_2 \end{bmatrix} ik - b \begin{bmatrix} Th_3 \end{bmatrix} = \mu \begin{bmatrix} M \end{bmatrix} k^2 + \mu \frac{b^2}{U^2} \begin{bmatrix} \omega \end{bmatrix}. \tag{2.46}$$

Multiply in N_w rows by $\frac{1}{b}$ and N_θ rows by $\frac{1}{b^2}$ and adopting a normalized variable $\frac{\eta}{b}$ thus effectively multiplying the N_w columns (left-hand) by b:

$$
-k^2\begin{bmatrix}[\Delta] & a[A]^T\\ a[A] & (a^2+\frac{1}{8})[\Delta]\end{bmatrix} - ik\begin{bmatrix}2C(k)[\delta] & -[1+2(\frac{1}{2}-a)C(k)][A]^T\\ 2(\frac{1}{2}+a)C(k)[A] & (\frac{1}{2}-a)[1-2(\frac{1}{2}+a)C(k)][\Delta]\end{bmatrix}
$$

$$
-\begin{bmatrix}[0] & -2C(k)[A]^T\\ [0] & -(1+2a)C(k)[\Delta]\end{bmatrix} = \mu k^2\begin{bmatrix}[\Delta] & -x_\theta[A]^T\\ -x_\theta[A] & r^2[\Delta]\end{bmatrix} + \mu\frac{b^2}{U^2}\begin{bmatrix}[\omega_{w_i}^2] & [0]\\ [0] & [r^2\omega_{\theta_i}^2]\end{bmatrix}. \tag{2.47}
$$

The frequency matrix can further be reduced by leveraging the ratio between successive modal frequency of a homogeneous cantilever beam and adopting σ as a variable representing the ratio of the 1st bending frequency over the 1st torsional frequency:

$$
\begin{bmatrix}[\omega_{w_i}^2] & [0]\\ [0] & [r^2\omega_{\theta_i}^2]\end{bmatrix} = \omega_{\theta_1}^2\begin{bmatrix}\sigma^2\left[\left(\frac{\alpha_i^2}{\alpha_1^2}\right)^2\right] & [0]\\ [0] & \left[r^2\left(\frac{\gamma_i}{\gamma_1}\right)^2\right]\end{bmatrix}. \tag{2.48}
$$

For notation purposes, let

$$
\begin{bmatrix}\sigma^2\left[\left(\frac{\alpha_i^2}{\alpha_1^2}\right)^2\right] & [0]\\ [0] & \left[r^2\left(\frac{\gamma_i}{\gamma_1}\right)^2\right]\end{bmatrix} = \Big[\Upsilon\Big]. \tag{2.49}
$$

Thus the complete flutter matrix (condensing equation 2.47) is of the form:

$$
\Big[F\Big] = \mu k^2\Big[\tilde{M}\Big] - k^2\Big[\tilde{Th}_1\Big] - ik\Big[\tilde{Th}_2(k)\Big] - \Big[\tilde{Th}_3(k)\Big] + \mu k^2\left(\frac{\omega_{\theta_1}}{\omega}\right)^2\Big[\Upsilon\Big], \tag{2.50}
$$

and the fundamental problem takes the form of:

$$\begin{bmatrix} F \end{bmatrix} \begin{bmatrix} \frac{\bar{\eta}}{b} \\ \bar{\zeta} \end{bmatrix} = \begin{bmatrix} 0 \end{bmatrix}. \tag{2.51}$$

For non-trivial solutions, we need $\det F = 0$. The typical technique for approaching such a problem is to specify the expected flight conditions (which constrains ρ_∞) and then specify a test range of k values. For each of these k values, the determinate equation yields multiple complex roots. These roots correspond to the number of mode shapes considered. In general these roots will be complex; however, at the flutter boundary one of these roots is expected to represent purely harmonic motion.

As one would expect, the K-method is limited in accuracy outside of purely harmonic motion [21]. However the method is still widely popular for its speed. Matlab implementation is included in appendix A.

Mode shapes and generalized coordinates are purely harmonic functions of time. Given this, behavior outside of harmonic motion ($g \neq 0$) should be carefully interpreted. However, considering the flutter boundary occurs when $g = 0$, this method is sufficiently accurate to calculate flutter speed and frequency.

2.4.2 PK-Method

The PK-Method is a hybrid amalgamation of the K and analytical P method, by which the aerodynamic behavior is still considered as purely a function of frequency, while the structural behavior is relaxed to include damped and un-damped behavior.

Once again starting from Hodges Equations 5.129 for the generalized forces using Theodorsen aerodynamics:

$$
\begin{Bmatrix} \Xi_w \\ \Xi_\theta \end{Bmatrix} = -\pi\rho_\infty b^2 l \begin{bmatrix} [\Delta] & ba[A]^T \\ ba[A] & b^2(a^2+\frac{1}{8})[\Delta] \end{bmatrix} \begin{bmatrix} \ddot{\eta} \\ \ddot{\zeta} \end{bmatrix}
$$

$$
-\pi\rho_\infty bUl \begin{bmatrix} 2C(k)[\delta] & -b[1+2(\frac{1}{2}-a)C(k)][A]^T \\ 2b(\frac{1}{2}+a)C(k)[A] & b^2(\frac{1}{2}-a)[1-2(\frac{1}{2}+a)C(k)][\Delta] \end{bmatrix} \begin{bmatrix} \dot{\eta} \\ \dot{\zeta} \end{bmatrix} \tag{2.52}
$$

$$
-\pi\rho_\infty bU^2 l \begin{bmatrix} [0] & -2C(k)[A]^T \\ [0] & -b(1+2a)C(k)[\Delta] \end{bmatrix} \begin{bmatrix} \eta \\ \zeta \end{bmatrix}.
$$

To condense notation take:

$$
\begin{Bmatrix} \Xi_w \\ \Xi_\theta \end{Bmatrix} = -\pi\rho_\infty b^2 l \begin{bmatrix} Th_1 \end{bmatrix} \begin{bmatrix} \ddot{\eta} \\ \ddot{\zeta} \end{bmatrix} - \pi\rho_\infty bUl \begin{bmatrix} Th_2 \end{bmatrix} \begin{bmatrix} \dot{\eta} \\ \dot{\zeta} \end{bmatrix} - \pi\rho_\infty bU^2 l \begin{bmatrix} Th_3 \end{bmatrix} \begin{bmatrix} \eta \\ \zeta \end{bmatrix}. \tag{2.53}
$$

The corresponding equations of motion form Hodges 5.130

$$
ml \begin{bmatrix} [\Delta] & -bx_\theta[A]^T \\ -bx_\theta[A] & b^2r^2[\Delta] \end{bmatrix} \begin{bmatrix} \ddot{\eta} \\ \ddot{\zeta} \end{bmatrix} + \begin{bmatrix} \frac{EI}{l^3}[B] & [0] \\ [0] & \frac{GJ}{l}[T] \end{bmatrix} \begin{bmatrix} \eta \\ \zeta \end{bmatrix} = \begin{Bmatrix} \Xi_w \\ \Xi_\theta \end{Bmatrix} \tag{2.54}
$$

$$
ml \begin{bmatrix} M \end{bmatrix} \begin{bmatrix} \ddot{\eta} \\ \ddot{\zeta} \end{bmatrix} + \begin{bmatrix} K \end{bmatrix} \begin{bmatrix} \eta \\ \zeta \end{bmatrix} = \begin{Bmatrix} \Xi_w \\ \Xi_\theta \end{Bmatrix}. \tag{2.55}
$$

Now, considering the generalized coordinates to be exponential functions (no longer strictly harmonic) of the form:

$$
\eta_i(t) = \bar{\eta}_i exp(\nu t) \tag{2.56}
$$

$$\zeta_i(t) = \bar{\zeta}_i exp(\nu t), \tag{2.57}$$

where $\nu = \frac{pU}{b}$, and where p is an unknown, dimensionless, complex eigenvalue. The differential terms become:

$$\dot{\eta}_i = \nu \bar{\eta}_i exp(\nu t), \qquad \dot{\zeta}_i = \nu \bar{\zeta}_i exp(\nu t),$$
$$\ddot{\eta}_i = \nu^2 \bar{\eta}_i exp(\nu t), \qquad \ddot{\zeta}_i = \nu^2 \bar{\zeta}_i exp(\nu t).$$

However, key to the PK method the generalized forces are maintained as pure functions of the the oscillatory frequency k, noting the relationship that $k = Imag(p)$. The equations of motion reduce to:

$$-\pi\rho_\infty b^2 l \begin{bmatrix} Th_1 \end{bmatrix} \nu^2 - \pi\rho_\infty bUl \begin{bmatrix} Th_2 \end{bmatrix} \nu - \pi\rho_\infty bU^2 l \begin{bmatrix} Th_3 \end{bmatrix} = ml \begin{bmatrix} M \end{bmatrix} \nu^2 + \begin{bmatrix} K \end{bmatrix}. \tag{2.58}$$

Multiplying all by $\frac{1}{\nu^2}$:

$$-\pi\rho_\infty b^2 l \begin{bmatrix} Th_1 \end{bmatrix} - \pi\rho_\infty bUl \begin{bmatrix} Th_2 \end{bmatrix} \frac{1}{\nu} - \pi\rho_\infty bU^2 l \begin{bmatrix} Th_3 \end{bmatrix} \frac{1}{\nu^2} = ml \begin{bmatrix} M \end{bmatrix} + \begin{bmatrix} K \end{bmatrix} \frac{1}{\nu^2}. \tag{2.59}$$

Using the definition of ν and further reduction:

$$-\pi\rho_\infty b^2 l\left[Th_1\right]-\pi\rho_\infty b^2 l\frac{1}{p}\left[Th_2\right]-\pi\rho_\infty b^3 l\frac{1}{p^2}\left[Th_3\right]=ml\left[M\right]+\frac{b^2}{p^2U^2}\left[K\right]. \quad (2.60)$$

Note that for a cantilever beam the stiffness matrix can be reduced in terms of modal frequencies:

$$[K]=ml\begin{bmatrix}[\omega_{w_i}^2] & [0] \\ [0] & b^2r^2[\omega_{\theta_i}^2]\end{bmatrix}=ml\left[\omega\right], \quad (2.61)$$

and incorporating this and further reduction also using the dimensionless mass ratio μ:

$$-\left[Th_1\right]-\frac{1}{p}\left[Th_2\right]-\frac{b}{p^2}\left[Th_3\right]=\mu\left[M\right]+\mu\frac{b^2}{p^2U^2}\left[\omega\right]. \quad (2.62)$$

Multiply in N_w rows by $\frac{1}{b}$ and N_θ rows by $\frac{1}{b^2}$ and adopting a normalized variable $\frac{\eta}{b}$ thus effectively multiplying the N_w columns (left-hand) by b:

$$-\begin{bmatrix}[\Delta] & a[A]^T \\ a[A] & (a^2+\frac{1}{8})[\Delta]\end{bmatrix}-\frac{1}{p}\begin{bmatrix}2C(k)[\delta] & -[1+2(\frac{1}{2}-a)C(k)][A]^T \\ 2(\frac{1}{2}+a)C(k)[A] & (\frac{1}{2}-a)[1-2(\frac{1}{2}+a)C(k)][\Delta]\end{bmatrix}$$
$$-\frac{1}{p^2}\begin{bmatrix}[0] & -2C(k)[A]^T \\ [0] & -(1+2a)C(k)[\Delta]\end{bmatrix}=\mu\begin{bmatrix}[\Delta] & -x_\theta[A]^T \\ -x_\theta[A] & r^2[\Delta]\end{bmatrix}+\mu\frac{b^2}{p^2U^2}\begin{bmatrix}[\omega_{w_i}^2] & [0] \\ [0] & [r^2\omega_{\theta_i}^2]\end{bmatrix}. \quad (2.63)$$

The frequency matrix can further be reduced by leveraging the ratio between successive modal frequency of a homogeneous cantilever beam and adopting σ as a variable representing the ratio of the 1st bending frequency over the 1st torsional frequency:

$$\begin{bmatrix} [\omega_{w_i}^2] & [0] \\ [0] & [r^2\omega_{\theta_i}^2] \end{bmatrix} = \omega_{\theta_1}^2 \begin{bmatrix} \sigma^2 \left[\left(\frac{\alpha_i^2}{\alpha_1^2} \right)^2 \right] & [0] \\ [0] & \left[r^2 \left(\frac{\gamma_i}{\gamma_1} \right)^2 \right] \end{bmatrix}. \tag{2.64}$$

For notation purposes, let

$$\begin{bmatrix} \sigma^2 \left[\left(\frac{\alpha_i^2}{\alpha_1^2} \right)^2 \right] & [0] \\ [0] & \left[r^2 \left(\frac{\gamma_i}{\gamma_1} \right)^2 \right] \end{bmatrix} = \left[\Upsilon \right]. \tag{2.65}$$

Thus the complete flutter matrix (condensing equation 2.63) is of the form:

$$\left[F \right] = \mu p^2 \left[\tilde{M} \right] - p^2 \left[T\tilde{h}_1 \right] - p \left[T\tilde{h}_2(k) \right] - \left[T\tilde{h}_3(k) \right] + \mu \left(\frac{b^2}{U^2} \right) \omega_{\theta_1}^2 \left[\Upsilon \right], \tag{2.66}$$

where the tilde denotes the new normalized matrices equation 2.63. And the fundamental problem takes the form of:

$$\left[F \right] \begin{bmatrix} \frac{\bar{\eta}}{b} \\ \bar{\zeta} \end{bmatrix} = \left[0 \right]. \tag{2.67}$$

For non-trivial solutions, we set $\det F = 0$, and solving this determinant equation will yield the sought solution set.

The solution technique implemented in appendix B is adopted from Hassig 1971. At a given set velocity U, we iteratively solve for p and k via the Regula Falsi method.

The PK method is considered to yield higher accuracy outside harmonic motion yet should perfectly agree with the K-method implementation at purely harmonic motion (which is the flutter boundary of an ideal un-damped system).

Chapter 3

IMPLEMENTATION

The following methods were applied to the case studies:

- K - Theodorsen (via assumed modes) [Current work MATLAB]
- PK - Theodorsen (via assumed modes) [Current work MATLAB]
- K - DLM (via assumed modes) [NASA EZASE]
- PKNL - DLM (finite element) [FEMAP NX NASTRAN AEROELASTICY PACKAGE]

The FEMAP NX NASTRAN aeroelasticity package is largely considered standard in contemporary industry and thus considered the highest fidelity method of those presented in this work. Other implementations are investigated for 1st order approximations of increasing complexity.

It was determined that modifying the EZASE code to implement a PK method was not worth the effort, given that critical results (at the flutter boundary) would yield identical results.

This chapter is divided into the following analysis sections:

- The Hodges base model to validate current work K and PK method
- A baseline flat-plate wing to bridge across finite element and K/PK methods of current the work

- The California Polytechnic State University - SLO (CP) 2020 to represent rib-strut balsa construction
- The University of Southern California (USC) 2020 to represent composite top spar structure

Student design teams (follow design cycles analogous to professional projects) thus a 1st order approximation of the K - Theodorsen method may be better suited for an early design study trade space as opposed to investing resources to implement a complete finite element method. The primary purpose of this work is to explore such a case.

3.1 Hodges Baseline

Hodges [1] includes a hypothetical reference example defined via normalized variables that is commonly considered standard in literature as a validation case for flutter analysis methods. This current work adopts the example to validate the K and PK methods originally written. Table 3.1 reproduces these wing parameters.

Parameter	Value
a	$-1/5$
e	$-1/10$
μ	20
r^2	6/25
σ	2/5

Table 3.1: Hodges wing parameters

Figure 3.1 is a plot of normalized velocity versus damping, commonly referred to as a "V-g" plot. Note that each line represents motion in its respective mode shape. This data can be queried for when $g = 0$. The damping constant crossing from negative to positive indicates that the system is becoming unstable, passing through purely harmonic motion at $g = 0$. This boundary defines the onset of flutter. Note that "real-world" systems commonly have an inherent amount of damping and thus this is a conservative estimation of the flutter speed. As a companion to the V-g plot, Figure 3.2 is a plot of normalized velocity versus frequency of each respective mode shape. Note how the two modes coalesce, a tale-tell sign of the modal coupling present during flutter conditions. Table 3.2 shows the quantitative results of this analysis, indicating excellent agreement between the application of the current K and PK methods with the reference literature.

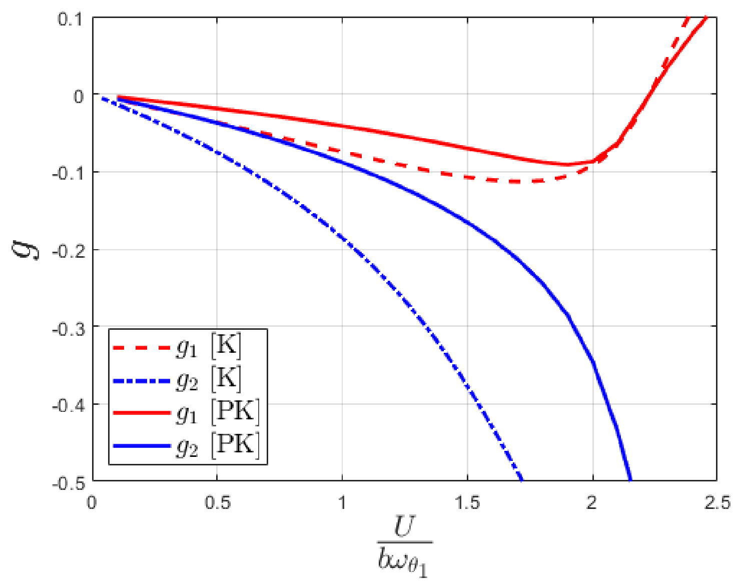

Figure 3.1: Hodges baseline V-g plot

	Reference[1]	K-Method	PK-Method	Relative Error
V_f	2.17	2.227	2.227	3%
ω_f/ω_θ	0.6443	0.638	0.638	1%

Table 3.2: Flutter results

3.1.0.1 Discussion

The Hodges baseline case proved out good agreement between published literature and the current work implementation of the K and PK methods. This case also demonstrates that the K and PK methods yield identical results at the conditions of

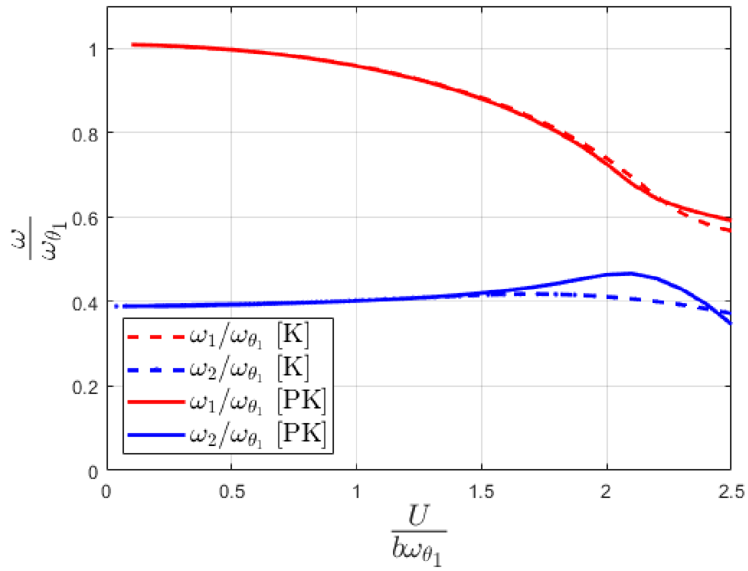

Figure 3.2: Hodges baseline V-ω plot

purely harmonic motion ($g = 0$). The slight variation from the reference is attributed to the approximation of Theodorsen's function used in the problem set from which the results were taken.

3.2 Plate-Wing Test Case

A further validation case was considered in both the current matlab codebase and the FEMAP NX NASTRAN Aeroelasticity package. It was then compared against the NASA EZASE code. The EZASE aluminum-like plate example is considered with dimensions 1 $[m]$ X 0.1 $[m]$ X 0.01 $[m]$, and aluminum-like material properties $E = 68.9e9$ $[Pa]$, $\nu = 0.4354$. Table 3.3 further defines the parameters of the plate wing. Preliminary to the flutter analysis, a modal analysis was performed with result summarized in table 3.4. Figure 3.3 shows the U-g plot of all methods considered, while figure 3.4 represents the corresponding frequency behavior. Qualitative results are summarized in table 3.5. Flutter speed is the critically important value, and the results of the K and PK methods are self-consistent and in good agreement ($\approx 5\%$) with the NASTRAN results, however the EZASE results appear offset ($\approx 10\%$) from these values. The various methods agree that the 1st torsional mode goes unstable and qualitatively follows the same behavior. Of secondary concern, frequency values are not in as good of quantitative agreement, however plot 3.4 shows qualitatively the various methods follow similar trends.

Parameter	Value
a	0
e	0
μ	280.63
r^2	0.33
c	0.10 $[m]$
L	1.00 $[m]$
GJ	749.60 $[Nm^2]$
EI	574.17 $[Nm^2]$
σ	0.263

Table 3.3: EZASE AL wing properties

Modal Frequency Analysis					
	TORSIONAL MODES			BENDING MODES	
	T1 [Hz]	**T2 [Hz]**	**B1 [Hz]**	**B2 [Hz]**	**B3 [Hz]**
NASTRAN	150.935	459.915	8.452	52.958	149.3008
Mechanics [MATLAB]	143.582	430.749	8.1603	51.1399	143.1934
% err	5%	6%	3%	3%	4%
EZASE	153.3775	463.0801	8.285	51.9146	145.651
% err	2%	1%	2%	2%	2%

Table 3.4: EZASE aluminum modal analysis

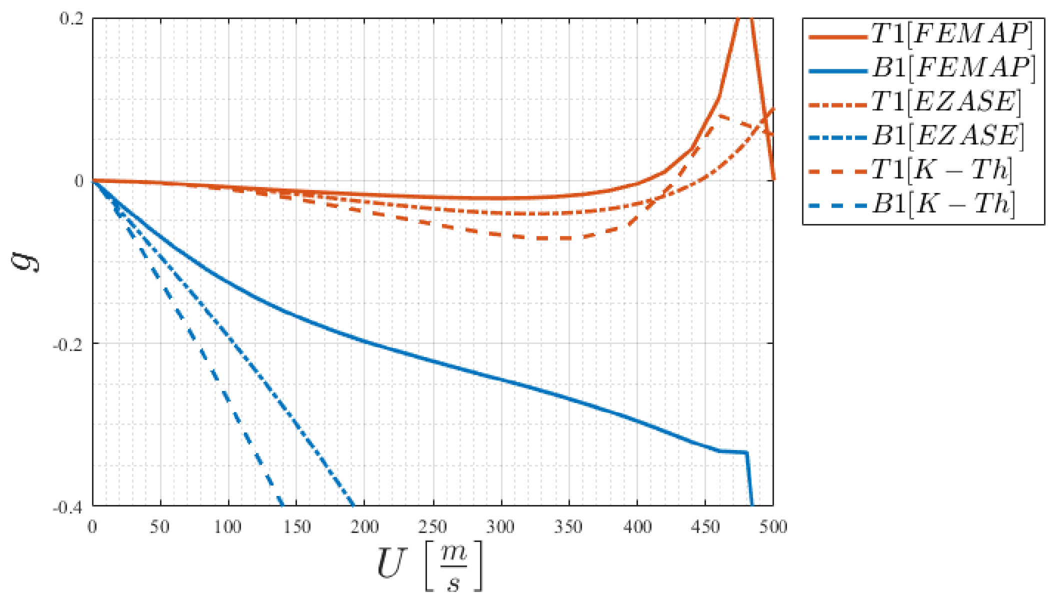

Figure 3.3: AL EZASE V-g plot

Flutter Results				
	U_F [m/s]	% err (rel. to NASTRAN)	ω_F [Hz]	% err
NASTRAN	405.93	-	108.3	-
K Method	428.08	5%	68.24	37%
PK Method	428.08	5%	68.24	37%
EZASE	445.72	10%	87.1	19%

Table 3.5: EZASE AL case flutter results

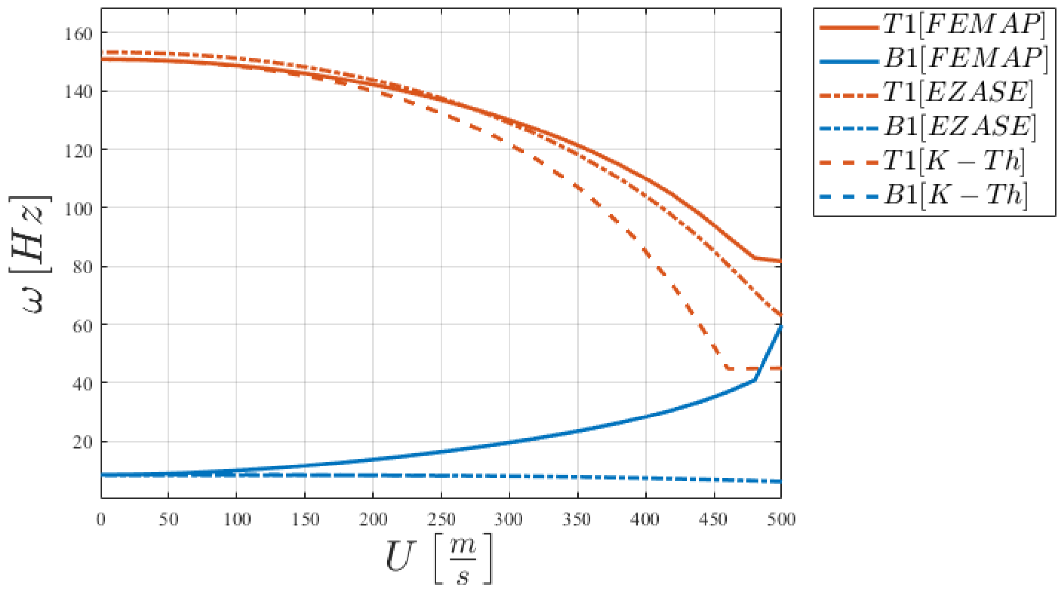

Figure 3.4: AL EZASE V-ω plot

3.2.0.1 Discussion

Four different methods were applied to the plate wing test case, each yielding results that differed non-negligibly. This case was initially considered with only the K, PK, and NASTRAN methods. Within this subset of results, it's obviously apparent that the flutter velocities were in near perfect alignment, although the flutter frequency posed significantly more deviation between the MATLAB and NASTRAN models. This disagreement served as motivation to seek a DLM implemented within MATLAB, leading to the adoption of the NASA EZASE code as an additional analysis method. The EZASE code links characteristics of the other methods, evaluating aerodynamic behavior via DLM (shared with NASTRAN), while maintaining a structural model more consistent with the current work's K, PK method implementation in MATLAB. However, the results from the EZASE code posed yet more questions. The flutter frequency showed improvement, but the flutter speed was out of agreement with previous NASTRAN and K, PK methods.

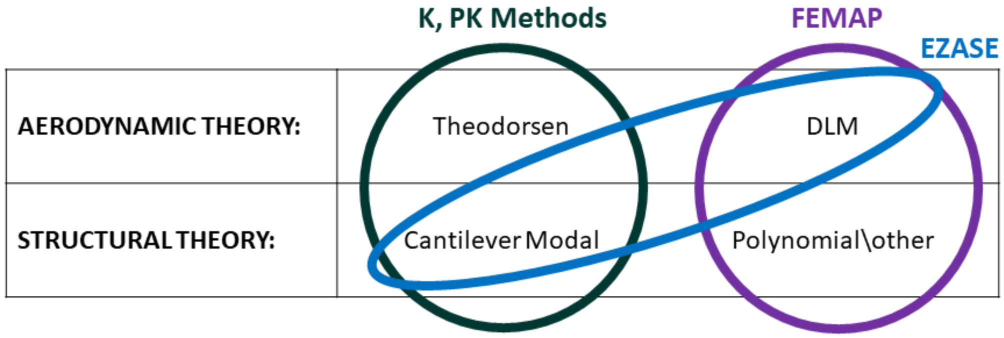

Figure 3.5: Link between underlying theories of analysis methods

A leading hypothesis is that this deviation is attributed to the use of polynomial structural mode shapes within the **N5KA** code [19]. This method, while more generalized, could deviate from the analytical mode shape solutions relevant to modeling a wing as a cantilever beam implemented within the other methods (current work MATLAB, and NASA EZASE). This would be a non-issue if a polynomial of sufficiently high order was considered within NASTRAN but such information must be held within the proprietary code. It's the author's working theory that this distinction between the methods may actually grow in magnitude during conditions of mode coupling at higher speeds, explaining how the frequency initially agrees at free vibration, 0 velocity. The relationship between analysis methods is layout in figure 3.5.

Chapter 4

RESULTS AND DISCUSSION

Based on the previous discussion of the implemented baseline cases, two methods were down selected for application to two DBF wings. The K-method was chosen for its speed and popularity as a preliminary design phase analysis [1]; additionally, a complete finite element model is built for detailed analysis within FEMAP NX Nastran Aeroelasticity package. Such a finite element method is largely considered industry standard and thus considered the highest fidelity results presented in this study in lieu of a practical wind tunnel testing. Each wing was selected to represent a class of construction methods typically adopted by university teams.

4.1 Spar-Rib Construction [Cal Poly - SLO 2020]

4.1.1 Results

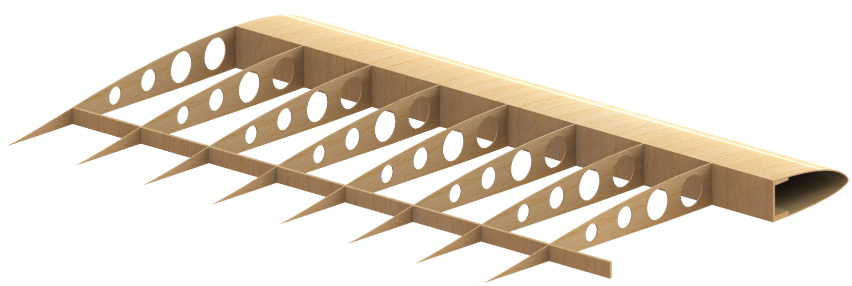

Figure 4.1: CP 2020 Wing

The Cal Poly SLO 2020 DBF wing is an example of spar-rib construction entirely made of balsa wood. While balsa wood has a wide range of material properties, those used in this study are included in table 4.3. Also important to note that with this interpretation, the balsa material is considered to instantaneously fail rather than yield. The wing characteristics are defined in table 4.1.

Modal analysis results are included in table 4.2, with depiction of the 1st bending and torsional modes in figure 4.2. First, a material failure case was considered. Done in reverse to the typically analysis, a maximum V_{ne} (Velocity Never-Exceed) was sought with an equivalent N-loading which generated the failure stress at the wings root given the established wing structure. The results of this static structural analysis are presented in figure 4.3. U-g and U-ω plots in figures 4.4 and 4.5 respectively. With a summary of results in table 4.4.

Parameter	Value
a	-0.48
e	-0.48
μ	0.68
r^2	0.1
c	0.5 $[m]$
L	0.762 $[m]$
GJ	552.9 $[Nm^2]$
EI	707.1 $[Nm^2]$
σ	0.263

Table 4.1: CP 2020 wing properties

As expected, the collocation of the elastic axis, center of gravity, and aerodynamic center limit the aeroelastic effects observed. The critically important V_{ne} is recognized during failure of the material in bending at the wing root. This case aligns with general DBF teams' assumption about neglecting aeroelastic behavior; however, such an analysis is still critical to consider given that "even when the mass and flexural axes are aligned with the aerodynamic center on the quarter chord, flutter can still occur" [8].

Modal Frequency Analysis						
	TORSIONAL MODES			BENDING MODES		
	T1[Hz]	**T2[Hz]**	**T3[Hz]**	**B1[Hz]**	**B2[Hz]**	**B3[Hz]**
Mechanics [MATLAB]	240.212	720.636	1201.06	63.35	397.058	1111.77
NASTRAN	240.2123	693.17	1135.65	61.38	348.1578	836.0672
% err	0%	4%	6%	3%	14%	33%

Table 4.2: CP 2020 modal analysis

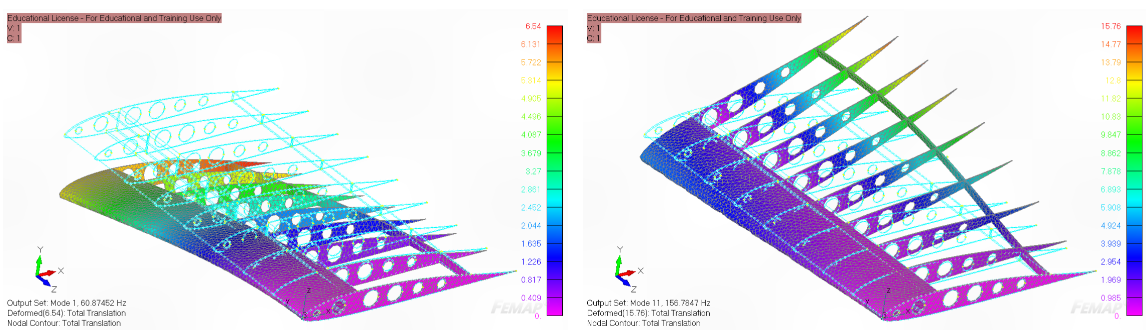

Figure 4.2: CP 2020 Mode shapes B1 (left) and T1 (right)

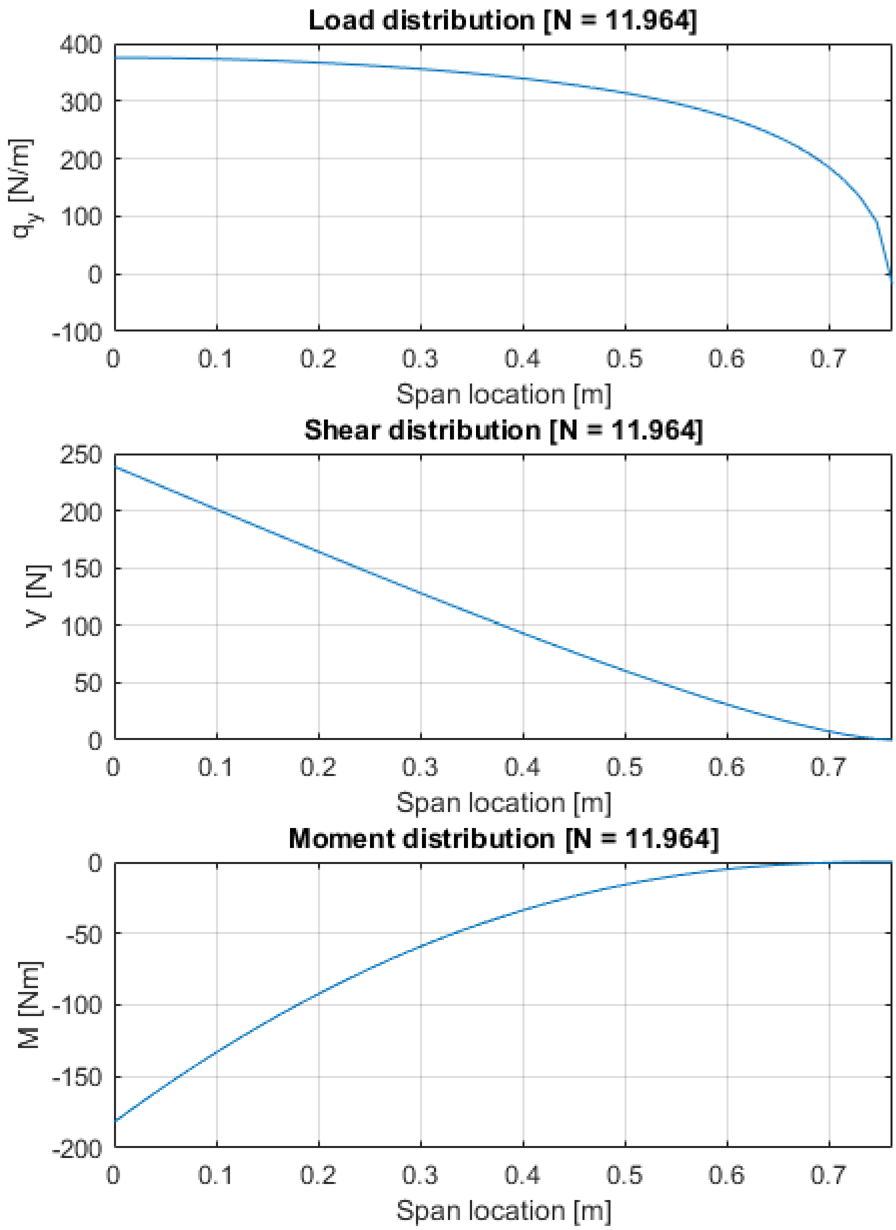

Figure 4.3: Load, shear, and moment distributions at failure via Prandtl lifting line theory (LLT)

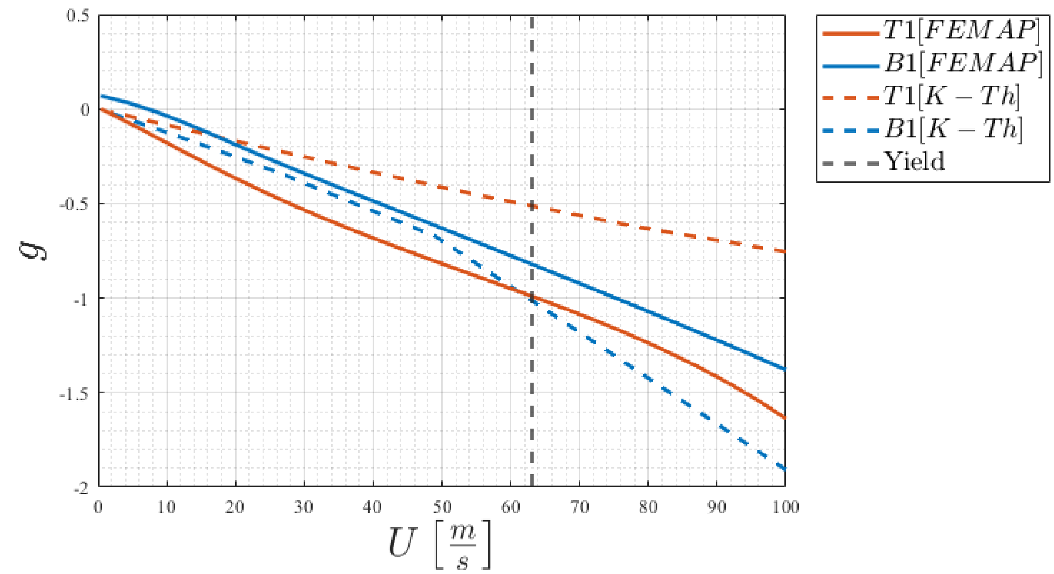

Figure 4.4: CP 2020 U-g plot dashed K-Theodorsen, solid NASTRAN

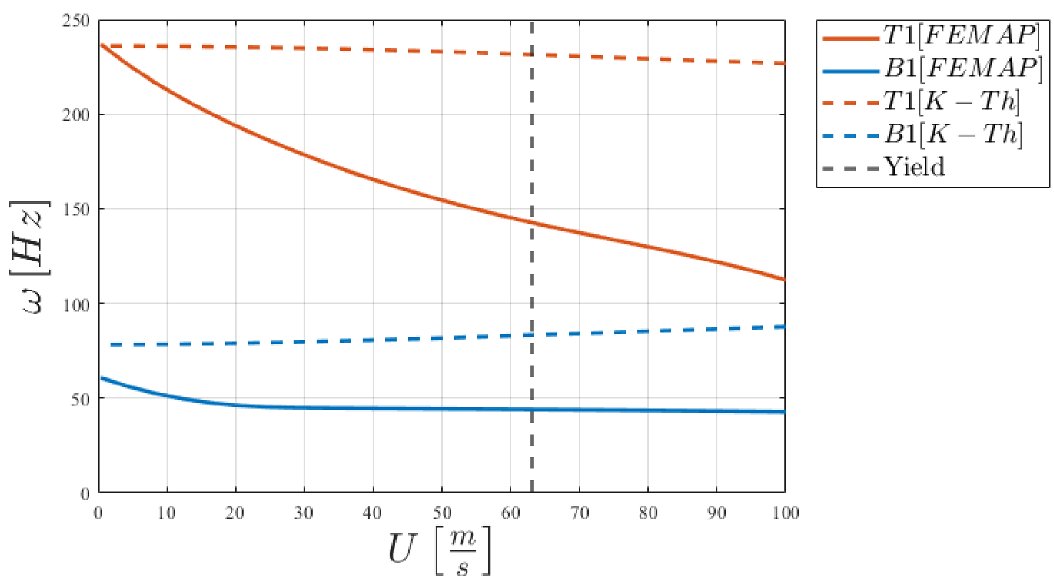

Figure 4.5: CP 2020 U-ω plot dsahed K-Theodorsen, solid NASTRAN

Parameter	Value
E	$3e9[Pa]$
ν	0.29
ρ	$160[kg/m^3]$

Table 4.3: Balsa wood material properties

V_{ne} **Summary**	
Static Aeroelastic	
Failure in Bending	
V [m/s]	N-equivalent
63.1	11.96
Torsional Divergence	
V [m/s]	
509	
Comment: Well beyond expected envelope	
Dynamic Aeroelastic	
Flutter [NX NASTRAN]	
V [m/s]	$\omega[Hz]$
-	-
Comment: Flutter behavior is not observed	

Table 4.4: CP 2020 V_{ne} results summary table

4.1.2 Discussion

The CP 2020 wing represents a spar-rib construction entirely composed of balsa wood. Emblematic of the co-location student philosophy, both the preliminary K-method analysis and higher fidelity finite element analysis did not indicate flutter behavior. This behavior is expected given that the general philosophy of collocating the aerodynamic center (CP), elastic axis (EA), and center of gravity (CG), generally weakens dynamic effects [22]. NASA TN D-3125, *A New Approach to the Explanation of the Flutter Mechanism*, lays out a distinctive catalog of flutter behavior types [22]. Although the parametric analysis presented in the NASA technical report was limited to 2D considerations, the case studies provide valuable context. Considering a typical section reduction of the CP 2020 wing, the collocation of the CP, CG, and EA does not explicitly match any of the categories; however, the behavior as evident in the NASTRAN results of figure 4.5 show the low frequency bending mode trends slightly down before settling at a potential pole, while the higher frequency torsional mode generally trends downward. This behavior could be analogous to case A3 consider in NASA TN D-3125, with the caveat that the torsional mode frequency trends inversely proportional with speed as opposed to proportional to it [22]. In a similar vein to the stability of case A3, a preliminary conclusion to draw from figures 4.5 and 4.4 is that the CP 2020 wing is stable (flutter is not expected before static structural failure). To emphasize that such a wing is not indestructible a static analysis is performed to determine the maximum loading lift distribution and the equivalent free stream speed which are otherwise typically set as requirements prior to wing design. Thus this aeroelastic analysis would leave the flight envelope, included as fig. 4.6 [2] unchanged.

Ultimately this analysis proved the stability of the particular CP 2020 wing model considered. This is not to say that all other such wings adopting the collocation strategy are likewise insusceptible to flutter. It remains theoretically possible for wing of such design to still exhibit flutter behavior [1].

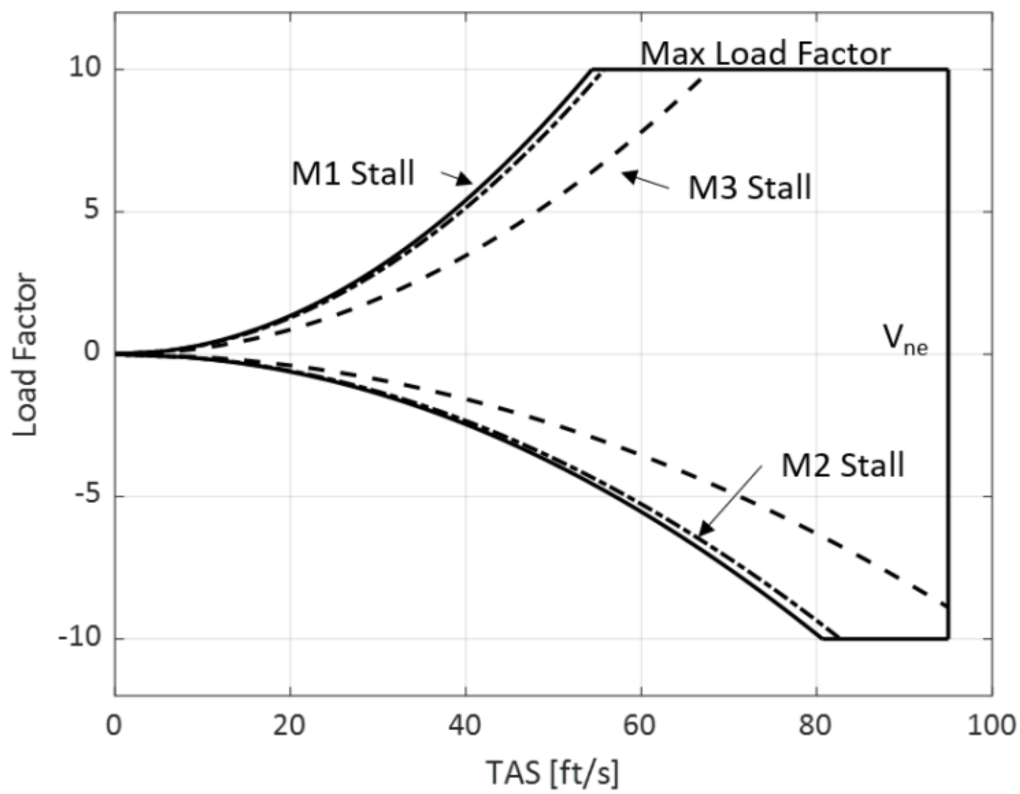

Figure 4.6: Cal Poly - SLO 2020 Envelope [2]

4.2 Single Top Composite Spar Cap [USC 2020]

4.2.1 Results

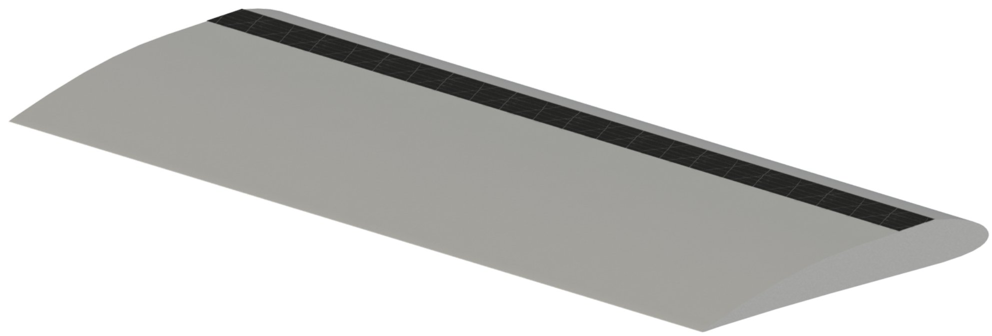

Figure 4.7: Composite single top spar (USC 2020)

The USC 2020 wing featured a single top spar composite plate a fixed to a foam airfoil volume. The top spar is made up of a stepped layered unidirectional carbon fiber. Each ply, estimated to be 0.01 $[in]$ thickness is step in a laminate from a 4-ply thickness from the root to 3 $[in]$ spanwise location, a 3 to 2 ply step at 8 $[in]$, an finally a 2 to 1 ply step at 14 $[in]$ location. Unidirectional standard carbon fiber is modeled as a 2D orthotropic material with properties summarized in table 4.6 [23]. Polyurethane foam material properties are summarized in table 4.7 [24].

Parameter	Value
a	-0.1538
e	-0.1636
μ	35.623
r^2	0.376
σ	0.199
c	0.304 $[m]$
L	0.70 $[m]$
ρIp	0.028

Table 4.5: USC 2020 wing properties

To build I_p and other relevant parameters for the k-method a typical cross section was considered of within the 3-ply region of the laminate. However, the ratio of fundamental frequencies σ was adopted from the NASTRAN modal analysis as an input into the k-method.

Parameter	Value
E_1	$1.35e11$ $[Pa]$
E_2	$1.00e10$ $[Pa]$
G	$5e9$ $[Pa]$
ν	0.3
ρ	1600 $[kg/m^3]$

Table 4.6: Standard unidirectional carbon fiber properties

In this case K-method and NASTRAN flutter prediction are in excellent agreement in both flutter speed and frequency.

4.2.2 Discussion

The USC 2020 wing, representative of a top spar composite construction did yield flutter behavior in both the k-method and NASTRAN finite element analysis methods. The flutter speed and frequency between these two methods were within 5% agreement. The typical section of the USC 2020 wing includes an EA slightly aft CG, which are both offset aft of the CP. This would fit into case B3a of the NASA TN D-3125 [22]. Figures 4.9 and 4.10 show indications of corresponding behavior with the frequencies of the mode shapes coalescing near flutter boundary.

Given that the flutter speed is beyond the incompressibility assumption, one might consider including transonic effects; however, such a study would be irrelevantly outside of expected flight conditions. Thus, while the wing was shown to exhibit flutter behavior, the analysis undertaken indicates flutter is not practically expected and therefore the wing should be stable within expected flight conditions. Surprising a flight envelope was not included within the USC 2020 Design Report, however the reported cruise speed $161 ft/s (49 m/s)$ is well below the determined flutter speed [25].

Parameter	Value
E	$7.4e8\ [Pa]$
ν	0.3
ρ	$425\ [kg/m^3]$

Table 4.7: Polyurethane foam properties

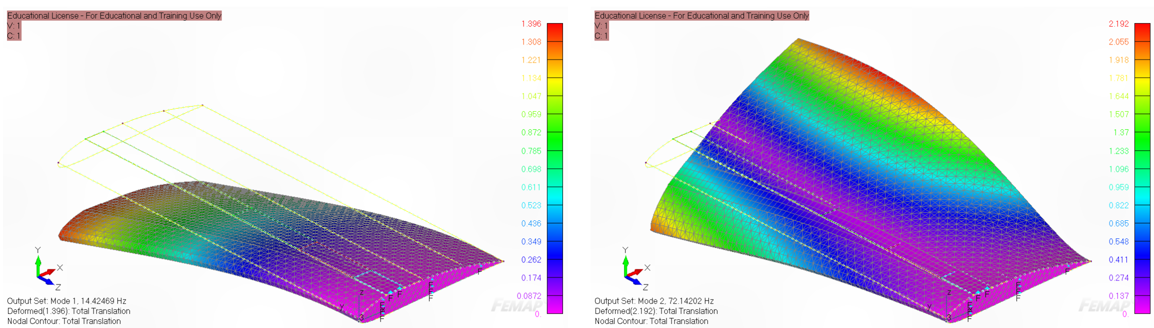

Figure 4.8: USC 2020 Mode shapes B1 (left) and T1 (right)

Modal Frequency Analysis			
	TORSIONAL MODES	BENDING MODES	
	T1 [Hz]	**B1 [Hz]**	**B2 [Hz]**
NASTRAN	72.14	14.42	86.21

Table 4.8: USC modal analysis summary

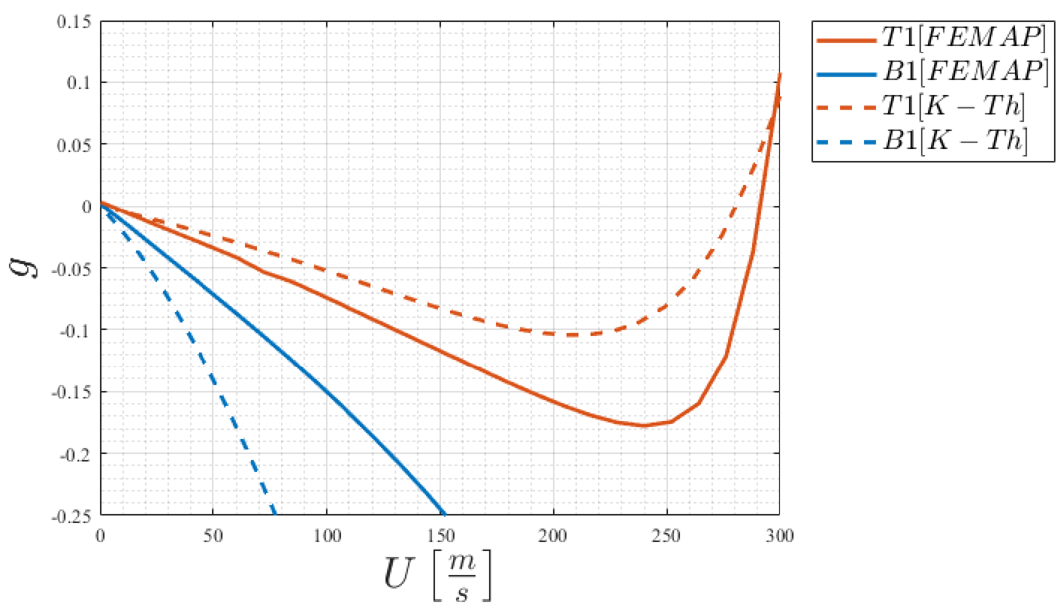

Figure 4.9: USC 2020 V-g plot dsahed K-Theodorsen, solid NASTRAN

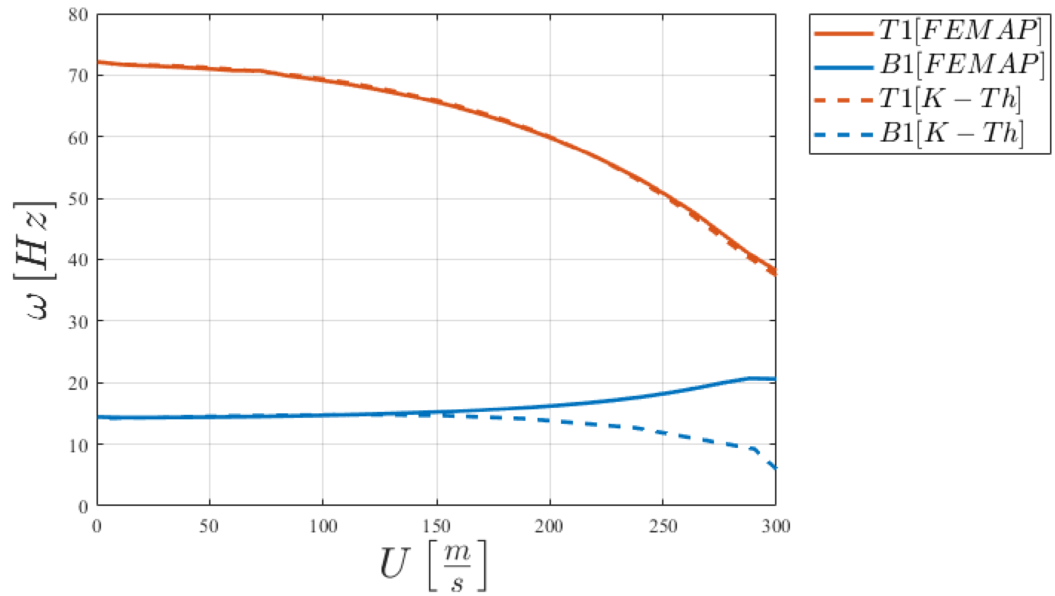

Figure 4.10: USC 2020 V-ω plot dsahed K-Theodorsen, solid NASTRAN

Flutter Results		
	U_F **[m/s]**	ω_F **[Hz]**
NASTRAN	291.045	40.223
K Method	280.33	42.384
% err	4%	5%

Table 4.9: USC 2020 flutter results summary

Chapter 5

FUTURE WORK

Physical wind tunnel testing is the ultimately authoritative truth for the determination of flutter speeds and frequencies. The application of code base and the other aeroelastic analysis methods to a wind tunnel study would be the logical next step of this work. The results would not only give insight into the slight discrepancies of the cases studied within the current work, but also serve as a keystone standard of all future aeroelastic studies at the university.

Additionally, the in-house codebase could be expanded to include more advanced aerodynamic and structural properties (considering wing sweep, dihedral angle, etc.), while additional value could also be added by considering body modes of the entire aircraft. These features would broadly expand the applicability of the analysis methods.

Within the context of DBF collegiate teams, the current work lays the foundation of a broader adoption of robust aeroelastic analyses in place of current rules of thumb, however a compiled stand-alone application resembling XFLR5 (a common tool used among groups for performance and stability simulations) would certainly encourage faster adoption. In the longer-term interest of developing such a tool, future graduate projects at Cal Poly - SLO could continue to expand the in-house code base while also expanding a reference library of previous DBF aircraft design aeroelastic characteristics.

Chapter 6

CONCLUSION

Small, lightweight aircraft are not immune from potentially catastrophic aeroelastic phenomena such as flutter and divergence. Within the context of DBF university teams, such dynamic analyses have often fallen a step short of consideration and in place, rules of thumb are adopted. This work surveyed a multitude of analysis methods for the determination of flutter speed, ranging from a K-method via assumed mode to bringing to bear the industry standard of a finite element method-based analysis via the NX NASTRAN FEMAP Aeroelasticity package, complete with doublet lattice aerodynamics.

Four distinctive flutter analysis methods were considered: the K method with Theodorsen aerodynamics, the PK method with Theodorsen aerodynamics, the K method with doublet lattice aerodynamics (DLM) via NASA EZASE code and the PKNL method with DLM aerodynamics (via NASTRAN). After validation of the in-house matlab code of the K and PK Theodorsen methods, all were applied to a validation plate wing case. The results of this case were in good agreement among subgroups of analysis approaches. While one may expect near perfect alignment between methods, further investigation found fundamental differences in the structural modal reduction of the various techniques, specifically between EZASE and NASTRAN. The application of both EZASE and NASTRAN to the same baseline plate-wing case was made in the interest of a purely apples-to-apples comparison; however, the results told a different story with the EZASE predicted flutter speed being an outlier of the otherwise excellent agreement of the other methods, and the flutter frequency middling the other predictions. As discussed in section 3.2.0.1, this difference is likely attributed to how the structural mode shapes are modeled. Recognizing this, the analysis methods were down selected to the K method with Theodorsen aerodynamics and NASTRAN for application to real wings flown in previous student projects.

The first DBF wing considered was the CP 2020. Representative of a typical box-spar balsa wood construction, this wing also notably featured a design strategy of collocation of the aerodynamic center (CP), elastic axis (EA), and center of masses (CG). In theory reducing the separation of all attributes generally reduces dynamic effective by shortening effectiveness moment arms. However, this strategy does not inherently eliminate flutter and divergence. In the CP 2020 case however, it was shown that this design was stable within the flight regime considered and would not exhibit any flutter behavior, especially at velocity below the V_{ne} dictated by material failure at the wing root.

The K-method proved more suitable for near homogeneous wings as evident by the excellent agreement of the flutter speed [$280.33m/s$] and frequency [$40.2Hz$] results of the USC 2020 wing model considered. Note that the flutter speed was beyond the bounds of typical flight conditions and approaching transonic conditions. While none of the methods consider a full treatment of transonic aerodynamics, the analysis as presented proves that flutter would not be expected within the incompressible flow regime assumption $M << 0.3 = 102m/s$. Although flutter behavior is predicted for this wing model and hence unstable, it is well outside of expected flight conditions, and thus the neglect of flutter considerations is retroactively justified.

With the caveat that a good wind tunnel test is worth a thousand expert opinions, this work surveyed two student project wing designs and determined that flutter was not expected within reasonable flight conditions. However, student teams designing aircraft such as those a part of the AIAA DBF competition should consider implementing more robust aeroelastic analysis methods in favor of generalized rules of thumb. Analytical methods such as the K-method in the present work are suitable for early design cycles, especially of fairly uniform wings. However, it is important to note that wings of more complex construction (such as a semi-dual spar composite) may not be accurately represented by such a method. At present, the highest fidelity aeroelastic analysis methods are finite element methods such as those included in the FEMAP NX NASTRAN aeroelasticity package. Such an analysis is suited for later phases of the design process.

BIBLIOGRAPHY

[1] Dewey H. Hodges and G. Alvin Pierce. *Introduction to Structural Dynamics and Aeroelasticity*, volume 15 of *Cambridge aerospace series*. Cambridge University Press, New York, 2011.

[2] Cal Poly DBF Team. 2020 DBF California Polytechnic State University Design Report, 2020.

[3] Raymond L. Bisplinghoff. *Aeroelasticity*. Addison-Wesley series in mechanics. Addison-Wesley PubCo, Cambridge, Mass., 1955.

[4] Advisory Group for Aerospace Research & Development. *Manual on Aeroelasticity (AGARD REPORT No. 578)*. Technical Editing and Reproduction Ltd Harford House, 1971.

[5] Marianna A. Shubov. Mathematical Modeling and Analysis of Flutter in Bending-Torsion Coupled Beams, Rotating Blades, and Hard Disk Drives. *Journal of Aerospace Engineering*, 17(2):56–69, April 2004.

[6] Y. C. Fung. *An introduction to the theory of aeroelasticity,*. Dover Publications, New York, 1969.

[7] Theodore Theodorsen. General Theory of Aerodynamic Instability and the Mechanism of Flutter. *NASA Ames Research Center Classical Aerodynamics Theory*, 1979.

[8] Jan R. Wright. *Introduction to aircraft aeroelasticity and loads*. Aerospace series. John Wiley & Sons Inc, Chichester, West Sussex, England, second edition. edition, 2015. Book Title: Introduction to aircraft aeroelasticity and loads.

[9] EZASE Easy Aeroelasticity: A Tool to Simulate Aircraft Wing Geometry(DRC-014-036) | NASA Software Catalog.

[10] C. C. Lin, E. Reissner, and H. S. Tsien. On Two-Dimensional Non-Steady Motion of a Slender Body in a Compressible Fluid. *Journal of Mathematics and Physics*, 27(1-4):220–231, 1948.

[11] John W. Miles. Linearization of the Equations of Non-Steady Flow in a Compressible Fluid. *Journal of Mathematics and Physics*, 33(1-4):135–143, 1954.

[12] M. Landahl, E. Mollo-Christensen, and Holt Ashley. Parametric Studies of Viscous and Non-Viscous Unsteady Flows. 1960.

[13] Bruce R. Munson, Donald F. Young, Theodore H. Okiishi, and Wade W. Huebsch. *A Brief Introduction To Fluid Mechanics, 5th Edition*. John Wiley & Sons, Inc., 5th edition edition, November 2010.

[14] Tomasz Wierzbick. Lecture 2: The Concept of Strain (PDF).

[15] John D. Anderson. *Fundamentals of aerodynamics*. McGraw-Hill series in aeronautical and aerospace engineering. McGraw Hill Education, New York, NY, sixth edition edition, 2017.

[16] Edward Albano and William P. Rodden. A doublet-lattice method for calculating lift distributions on oscillating surfaces in subsonic flows. *AIAA Journal*, 7(2):279–285, February 1969. Publisher: American Institute of Aeronautics and Astronautics.

[17] Max Blair. A Compilation of the Mathematics Leading to the Doublet Lattice Method. Technical report, WRIGHT LAB WRIGHT-PATTERSON AFB OH, March 1992. Section: Technical Reports.

[18] Ben Names. *An Efficient Reduced Order Modeling Method for Analyzing Composite Beams Under Aeroelastic Loading*. PhD thesis, Virginia Polytechnic Institute and State University, April 2016.

[19] Rudy Yurkovich. Status of Unsteady Aerodynamic Prediction for Flutter of High-Performance Aircraft. *Journal of Aircraft*, 40(5):832–842, September 2003. Publisher: American Institute of Aeronautics and Astronautics.

[20] Joseph P. Giesing, Terez P. Kalman, and William P. Rodden. Subsonic Unsteady Aerodynamics for General Configurations. Part 2. Volume 2. Computer Program N5KA. Technical report, DOUGLAS AIRCRAFT CO LONG BEACH CA, April 1972. Section: Technical Reports.

[21] Hermann J. Hassig. An approximate true damping solution of the flutter equation by determinant iteration. *Journal of Aircraft*, May 2012.

[22] M. H. Rheinfurth and F. W. Swift. A new approach to the explanation of the flutter mechanism. Technical Report NASA-TN-D-3125, January 1966. NTRS Author Affiliations: NASA Marshall Space Flight Center NTRS Document ID: 19660006195 NTRS Research Center: Legacy CDMS (CDMS).

[23] Mechanical Properties of Carbon Fibre Composite Materials.

[24] Overview of materials for Thermoset Polyurethane Foam, Unreinforced.

[25] USC DBF Team. 2020 DBF University of Southern California Design Report, 2020.

[26] Charles Goodman. Accurate Subcritical Damping Solution of Flutter Equation Using Piecewise Aerodynamic Function. *Journal of Aircraft*, 38(4):755–763, July 2001.

[27] Richard Bauer and Austin Hardman. Fin Flutter Analysis. *Aerospace Engineering*, June 2013.

[28] Various DBF Teams. "AIAA Design, Build, Fly Previous Competitions" 2015-2020.

[29] Fact Sheet – Small Unmanned Aircraft Systems (UAS) Regulations (Part 107). Type: template.

[30] John W. Edwards and Carol D. Wieseman. Flutter and Divergence Analysis Using the Generalized Aeroelastic Analysis Method. *Journal of Aircraft*, 45(3):906–915, May 2008.

[31] William P. Rodden and Bernhard Stahl. A strip method for prediction of damping in subsonic wind tunnel andflight flutter tests. *Journal of Aircraft*, 6(1):9–17, January 1969.

[32] Walter A. Silva, Pawel Chwalowski, and Boyd N. Perry. Evaluation of Linear, Inviscid, Viscous, and Reduced-Order Modeling Aeroelastic Solutions of the AGARD 445.6 Wing Using Root Locus Analysis. In *55th AIAA/ASME/ASCE/AHS/ASC Structures, Structural Dynamics, and Materials Conference*. American Institute of Aeronautics and Astronautics.

[33] M Goland. The Flutter of a Uniform Cantilever Wing. *Journal of Applied Mechanics*, 12(4):A197–A208, December 1945.

[34] Robert H Scanlan and R. A Rosenbaum. *Introduction to the study of aircraft vibration and flutter*. Dover Publications, New York, 1968.

[35] Carlos Cesnik, Dewey Hodges, and Mayuresh Patil. Aeroelastic analysis of composite wings. In *37th Structure, Structural Dynamics and Materials Conference*,

Structures, Structural Dynamics, and Materials and Co-located Conferences. American Institute of Aeronautics and Astronautics, April 1996.

[36] T. P. Kalman, W. P. Rodden, and J. P. Giesing. Application of the Doublet-Lattice Method to Nonplanar Configurations in Subsonic Flow. *Journal of Aircraft*, 8(6):406–413, June 1971. Publisher: American Institute of Aeronautics and Astronautics.

[37] An approximate true damping solution of the flutter equation by determinant iteration. | Journal of Aircraft.

APPENDICES

Appendix A

K-METHOD.M

```
% AEROELASTIC ANALYSIS
% K-METHOD
% [Kent Roberts 2020-2021]

clear all;

%% Wing Definition (Unifrom)
%[HODGES]
a = -1/5;
e = -1/10;
x_theta = e - a;
rSquared = 6/25;
mu = 20;
sigma = 2/5;

%% FLUTTER K METHOD

% Specify number of assumed modes in bending and torsion
N_w = 1;
N_theta = 1;

% ===== Equations of Motion =====
% [Hodges 5.130]

% Create off-diagnoal matrix A
A = zeros(N_theta, N_w);

% Build coupling matrix
for i=1:N_theta
    phi = @(x) sin(GAMMAil(i)*x);

    for j=1:N_w

        beta = (cosh(ALPHAil(j))+cos(ALPHAil(j)))...
        /(sinh(ALPHAil(j))+sin(ALPHAil(j)));

        psi = @(x) cosh(ALPHAil(j)*x) - ...
           cos(ALPHAil(j)*x) ...
            - beta*(sinh(ALPHAil(j)*x) - ...
              sin(ALPHAil(j)*x));

        A(i,j) = integral(@(x)phi(x).*psi(x),0,1);
    end
end

```

```
M = mu*[eye(N_w)...
    -x_theta*A';...
    -x_theta*A...
    rSquared*eye(N_theta)/2]; %/2

%% ===== Generalized Forces =====
C = @(k) besselh(1,2,k) / ...
   (besselh(1,2,k)+1i*besselh(0,2,k));

Th1 = -[eye(N_w),...
       a*A';...
       a*A,...
       (a^2 + (1/8))*eye(N_theta)/2];%/2

Th2 = @(k) -(1i/k)*[2*C(k)*eye(N_w),...
                    -(1 + 2*(0.5 - a)*C(k))*A';...
                    2*(0.5+a)*C(k)*A,...
            (0.5-a)*(1-2*(0.5+a)*C(k))*eye(N_theta)/2];%/2

Th3 = @(k) -(1/ k^2)*[zeros(N_w),...
                        -2*C(k)*A';...
                        zeros(N_theta,N_w),...
                        -(1+2*a)*C(k)*eye(N_theta)/2];%/2

%% Sigma2 matrix

B_wi = zeros(N_w);
for i = 1:N_w
    B_wi(i,i) = (ALPHAil(i)/ALPHAil(1))^4;
end

T_wi = zeros(N_theta);
for i = 1:N_theta
    T_wi(i,i) = (GAMMAil(i)/GAMMAil(1))^2;
end


Sigma2 = [sigma^2 * B_wi,...
          zeros(N_w,N_theta);...
          zeros(N_theta, N_w),...
          T_wi];

%define Z to be complex, (w_theta_1/w)^2 * (1+ig)
syms Z
Z_mat = [eye(N_w)*Z...
        zeros(N_w,N_theta);...
        zeros(N_theta,N_w)...
        eye(N_theta)*Z*rSquared/2]; %ADDED /2

%% K-Method
K_min = 0.01;
K_max = 2;
N = 200;

K = [linspace(K_min,K_max,N-2),5,10];

% Create array to store solutions
X = zeros(N_w+N_theta, N);

for i = 1:length(K)
```

```
    Flutter_Matrix = M - Th1 + Th2(K(i)) +Th3(K(i)) - ...
       mu*Sigma2*Z_mat;

    X(:,i) = double(vpasolve(det(Flutter_Matrix)==0,Z));

    fprintf("%i %% \n",round((i/N)*100));
end


%% FLutter Output

% Create arrays for frequencies, damping, and reduced ...
   speed
omegaOverOmegaTheta1 = zeros(N_w+N_theta, N);
g = zeros(N_w+N_theta, N);
V = zeros(N_w+N_theta, N);
X_i = zeros(N_w+N_theta, N);
X_r = zeros(N_w+N_theta, N);


parfor i=1:N_w+N_theta
    X_i(i,:) = imag(X(i,:));
    X_r(i,:) = real(X(i,:));
    omegaOverOmegaTheta1(i,:) = 1./sqrt(real(X(i,:)));
    g(i,:) = imag(X(i,:))./real(X(i,:));
    V(i,:) = 1./(K.*sqrt(real(X(i,:))));
end

%V-omega plot

figure(1)
hold on

for i=1:N_w+N_theta
    if i==1
        plot(V(i,:), omegaOverOmegaTheta1(i,:), ...
           'r--','LineWidth',2)
        grid on
        xlabel('$\frac{U}{b \omega_{\theta_1}}$', ...
           'interpreter','latex','FontSize',22)
        ylabel('$ \frac{\omega}{\omega_{\theta_1}}$', ...
           'interpreter','latex','FontSize',22)
    elseif i==2
        plot(V(i,:), omegaOverOmegaTheta1(i,:), ...
           'b--.','LineWidth',2)
        legend('$ \omega_1/\omega_{\theta_1}$ [K]', ...
           '$ \omega_2/\omega_{\theta_1}$ ...
           [K]','interpreter','latex','Location',...
        'eastoutside','FontSize',14)
    end
end
xlim([0 2.5])
hold off

%% V-g plot

figure(2)
hold on

for i=1:N_w+N_theta
```

```
    if i==1
        plot(V(i,:), g(i,:), 'r--','LineWidth',2)
        grid on
        xlabel('$\frac{U}{b \omega_{\theta_1}}$', ...
              'interpreter','latex','FontSize',22)
        ylabel('$ g$', ...
              'interpreter','latex','FontSize',22)
    elseif i==2
        plot(V(i,:), g(i,:), 'b-.','LineWidth',2)
        legend('$g_1$ [K]','$g_2$ ...
              [K]','interpreter','latex','Location'...
        ,'eastoutside','FontSize',14)
    end
end
xlim([0 2.5])
hold off
```

Appendix B

PK-METHOD.M

```
% AEROELASTIC ANALYSIS
% PK-METHOD
% [Kent Roberts 2020-2021]

clear all;

%% Wing Definition (Unifrom)
%[HODGES]
a = -1/5;
e = -1/10;
x_theta = e - a;
rSquared = 6/25;
mu = 20;
sigma = 2/5;

%% FLUTTER PK METHOD

% Specify number of assumed modes in bending and torsion
N_w = 1;
N_theta = 1;

nat_freq = zeros(1,N_w+N_theta); %used for initial p ...
   guess
for i = 1:N_w
    nat_freq(i) = sigma * (ALPHAil(i)/ALPHAil(1))^2;
end
for i = N_w+1:N_w+N_theta
    nat_freq(i) = (GAMMAil(i)/GAMMAil(1));
end

% Create off-diagnoal matrix A
A = zeros(N_theta, N_w);

% Build coupling matrix
for i=1:N_theta
    phi = @(x) sin(GAMMAil(i)*x);

    for j=1:N_w

        beta = (cosh(ALPHAil(j))+cos(ALPHAil(j)))/...
        (sinh(ALPHAil(j))+sin(ALPHAil(j)));

        psi = @(x) cosh(ALPHAil(j)*x) - ...
           cos(ALPHAil(j)*x) ...
            - beta*(sinh(ALPHAil(j)*x) - ...
               sin(ALPHAil(j)*x));

        A(i,j) = integral(@(x)phi(x).*psi(x),0,1);
    end
```

```
end

M = mu*[eye(N_w)...
    -x_theta*A';...
    -x_theta*A...
    rSquared*eye(N_theta)/2]; %/2

%% ===== Generalized Forces =====
% [Hodges 5.129]
% Theodorsen
C = @(k) besselh(1,2,k) / ...
   (besselh(1,2,k)+1i*besselh(0,2,k));

Th1 = -[eye(N_w),...
       a*A';...
       a*A,...
       (a^2 + (1/8))*eye(N_theta)/2];%/2

Th2 = @(k) -[2*C(k)*eye(N_w),...
            -(1 + 2*(0.5 - a)*C(k))*A';...
            2*(0.5+a)*C(k)*A,...
            (0.5-a)*(1-2*(0.5+a)*C(k))*eye(N_theta)/2];%/2

Th3 = @(k) -[zeros(N_w),...
            -2*C(k)*A';...
            zeros(N_theta,N_w),...
            -(1+2*a)*C(k)*eye(N_theta)/2];%/2

%% Sigma2 matrix
B_wi = zeros(N_w);
for i = 1:N_w
    B_wi(i,i) = (ALPHAil(i)/ALPHAil(1))^4;
end

T_wi = zeros(N_theta);
for i = 1:N_theta
    T_wi(i,i) = (GAMMAil(i)/GAMMAil(1))^2;
end

Sigma2 = [sigma^2 * B_wi,...
          zeros(N_w,N_theta);...
          zeros(N_theta, N_w),...
          T_wi*rSquared/2];
%% PK-Method

Flutter_Matrix = @(p,k,V) (p^2)*(M) - (p^2)*(Th1) - ...
   p*(Th2(k)) - Th3(k)...
    +mu*(1 / (V^2))*(Sigma2);

syms p

V_arr = 0.1:0.1:5; %velocities [m/s]

N_end = length(V_arr) * (N_w+N_theta);

for i = 1:length(V_arr) %for each speed
    for j = 1:N_w+N_theta %for each mode shape
        if i == 1 %first speed specificied, build ...
           first guess based on nat. freq
            %[HASSIG 1971]
            F = 0.01;
```

```
            G = 1;
            p(j,2) = 0 + 1i*(nat_freq(j)/V_arr(i));%0 ...
               + 1i*(nat_freq(j)*b/V_arr(i));
            p(j,1) = -F*imag(p(j,2)) + 1i*G*imag(p(j,2));
            n = 2;
        else
            %build from last
            p(j,1) = (V_arr(i-1)/V_arr(i))*p(j,2);
            p(j,2) = (V_arr(i-1)/V_arr(i))*pc(j,i-1);
            n = 2;
        end

        %1st itr for loop condition

        while n≤20 %set max iteration
            F_det(j,n-1) = ...
               vpa(det(Flutter_Matrix(p(j,n-1),...
            imag(p(j,n-1)),V_arr(i))));
            F_det(j,n) = ...
               vpa(det(Flutter_Matrix(p(j,n),...
            imag(p(j,n)),V_arr(i))));

            if abs(norm((F_det(j,n-1)-F_det(j,n)))) < ...
               1e-5 %tolerance
                break;
            end

            if n == 20
                disp("max itr")
            end

            p(j,n+1) = (p(j,n)*F_det(j,n-1) - ...
               p(j,n-1)*F_det(j,n))...
            /(F_det(j,n-1)-F_det(j,n)); %Reglua Falsi ...
               [Hassig]

            n = n+1;
        end
        %save converged values
        pc(j,i) = p(j,n);

        %status
        status = 100*(((i-1)*(N_w+N_theta) + j) / N_end);
        fprintf('%i %% \n',round(status));
    end
end

%% post process
[pc_r, pc_c] = size(pc);

for i = 1:pc_r
    for j = 1:pc_c
        w(i,j) = imag(pc(i,j))*V_arr(j);
    end
end

w_norm = w;

for i = 1:pc_r
    for j = 1:pc_c
```

```
        if imag(pc(i,j)) == 0
            gamma(i,j) = real(pc(i,j))*1000; %instead of dividing by 0
        else
            gamma(i,j) = real(pc(i,j))/imag(pc(i,j));
        end
    end
end

V = V_arr;

%% plot

figure(1)
hold on

plot(V,w_norm,'LineWidth',2)

grid on
xlim([0 2.5])
ylim([0 1.1])

xlabel('$\frac{U}{b \omega_{\theta_1}}$', 'interpreter','latex','FontSize',22)
ylabel('$ \frac{\omega}{\omega_{\theta_1}}$', 'interpreter','latex','FontSize',22)
legend('$ \omega_1/\omega_{\theta_1}$ [K]', '$ \omega_2/\omega_{\theta_1}$ [K]','$ \omega_1/\omega_{\theta_1}$ [PK]', '$ \omega_2/\omega_{\theta_1}$ [PK]','interpreter','latex',...
'Location','eastoutside','FontSize',14)
%title('PLATE WING: Freq. Plot (PK-method)')

%% Gamma
figure(2)
hold on

plot(V,gamma,'LineWidth',2)

grid on
xlim([0 2.5])
ylim([-1 1])

xlabel('$\frac{U}{b \omega_{\theta_1}}$', 'interpreter','latex','FontSize',22)
ylabel('$ g$', 'interpreter','latex','FontSize',22)
legend('$g_1$ [K]','$g_2$ [K]','$g_1$ [PK]','$g_2$ [PK]','interpreter','latex','Location',...
'eastoutside','FontSize',14)
ylim([-0.5,0.1])
xlim([0,2.5])
%title('PLATE WING: Vg Plot (PK-method)')

%% HODGES FIG 5.22
GAMMA_w_th = real(pc.*V_arr);
xlim([0 2.5])

figure()
hold on
```

```
plot(V,GAMMA_w_th,'LineWidth',2)

grid on
xlim([0 2.5])
```